Development of a Family of Ultra-High Performance Concrete Pi-Girders

December 2013

NTIS Accession No. PB2014-100626

FHWA Publication No. FHWA-HRT-14-027

U.S. Department of Transportation
Federal Highway Administration

FOREWORD

With the ever increasing congestion and deterioration of our nation's highway system, a need exists to develop highly durable and rapidly constructed infrastructure systems. Durable bridge structures that would require less intrusive maintenance and would exhibit longer life spans thus maximizing the use of the facility are highly desirable. Expediting bridge construction can minimize traffic flow disruptions. Ultra-high performance concrete (UHPC) is an advanced construction material which affords new opportunities to envision the future of the highway infrastructure. The Federal Highway Administration has been engaged in research into the optimal uses of UHPC in the highway bridge infrastructure since 2001 through its Bridge of the Future Initiative. This report presents the results of a research effort aimed at engaging the finite element method as a means to facilitate the development of UHPC structural systems. In this study, a commercial finite element analysis package is used to develop a series of finite element optimized UHPC pi-girder sections for short and median bridge spans according to the requirements of AASHTO. The UHPC material model is based on the concrete damage plasticity theory and has been previously calibrated through several full-scale physical experiments.

This report corresponds to the TechBrief titled, "Development of a Family of Ultra-High Performance Concrete Pi-Girders" (FHWA-HRT-14-028). This report is being distributed through the National Technical Information Service for informational purposes. The content in this report is being distributed "as is" and may contain editorial or grammatical errors.

TECHNICAL REPORT DOCUMENTATION PAGE

1. Report No.
FHWA-HRT-14-027

2. Government Accession No.
NTIS PB2014-100626

3. Recipient’s Catalog No.

4. Title and Subtitle
Development of a Family of Ultra-High Performance Concrete Pi-Girders

5. Report Date
December 2013

6. Performing Organization Code:

7. Author(s)
Gang Zhang, Benjamin Graybeal, and Linfeng Chen

8. Performing Organization Report No.

9. Performing Organization Name and Address
Office of Infrastructure Research & Development
Federal Highway Administration
6300 Georgetown Pike
McLean, VA 22101-2296

10. Work Unit No.

11. Contract or Grant No.

12. Sponsoring Agency Name and Address
Office of Infrastructure Research & Development
Federal Highway Administration
6300 Georgetown Pike
McLean, VA 22101-2296

13. Type of Report and Period Covered
Final Report: 2008-2013

14. Sponsoring Agency Code
HRDI-40

15. Supplementary Notes
This document was developed by research staff at the Turner-Fairbank Highway Research Center. Portions of the work were completed by PSI, Inc. under contract DTFH61-10-D-00017. Gang Zhang and Linfeng Chen of PSI, Inc., and Ben Graybeal of FHWA, who manages the FHWA Structural Concrete Research Program, developed this document.

16. Abstract
Ultra-high performance concrete (UHPC) is an advanced cementitious composite material which has been developed in recent decades. When compared to more conventional cement-based concrete materials, UHPC tends to exhibit superior properties such as increased durability, strength, and long-term stability. Past research and deployment efforts have demonstrated that the pi-girder concept is viable from the structural design, fabrication, and construction standpoints. This computational investigation focused on developing a series of finite element optimized sections of UHPC pi-girders to effectively utilize the superior mechanical properties of UHPC over longer span lengths. The research was performed using the previously calibrated concrete damage plasticity model to represent the elastic and plastic response of the UHPC in the numerical simulation. The new cross-sections were developed based on the 2nd generation pi-girder that was previously tested in the laboratory. The cross-sectional parameters that were modified include girder depth, bulb width and height, web thickness, and the number of strands in the bulb. The analysis evaluated the local transverse bending capacity of the deck, the global flexural and shear capacity, and the deflection of the girder. Four cross sections with depths between 35 and 47 inches facilitating spans up to 135 feet are presented.

This report corresponds to the TechBrief titled “Development of a Family of Ultra-High Performance Concrete Pi-Girders” (FHWA-HRT-14-028).

17. Key Words
Ultra-high performance concrete, UHPC, finite element analysis, Pi-Girder, Structural optimization

18. Distribution Statement
No restrictions. This document is available through the National Technical Information Service, Springfield, VA 22161.

19. Security Classif. (of this report)
Unclassified

20. Security Classif. (of this page)
Unclassified

21. No. of Pages
58

22. Price
N/A

Form DOT F 1700.7 (8-72) Reproduction of completed page authorized

SI* (MODERN METRIC) CONVERSION FACTORS

APPROXIMATE CONVERSIONS TO SI UNITS

Symbol	When You Know	Multiply By	To Find	Symbol
		LENGTH		
in	inches	25.4	millimeters	mm
ft	feet	0.305	meters	m
yd	yards	0.914	meters	m
mi	miles	1.61	kilometers	km
		AREA		
in^2	square inches	645.2	square millimeters	mm^2
ft^2	square feet	0.093	square meters	m^2
yd^2	square yard	0.836	square meters	m^2
ac	acres	0.405	hectares	ha
mi^2	square miles	2.59	square kilometers	km^2
		VOLUME		
fl oz	fluid ounces	29.57	milliliters	mL
gal	gallons	3.785	liters	L
ft^3	cubic feet	0.028	cubic meters	m^3
yd^3	cubic yards	0.765	cubic meters	m^3
		NOTE: volumes greater than 1000 L shall be shown in m^3		
		MASS		
oz	ounces	28.35	grams	g
lb	pounds	0.454	kilograms	kg
T	short tons (2000 lb)	0.907	megagrams (or "metric ton")	Mg (or "t")
		TEMPERATURE (exact degrees)		
°F	Fahrenheit	5 (F-32)/9 or (F-32)/1.8	Celsius	°C
		ILLUMINATION		
fc	foot-candles	10.76	lux	lx
fl	foot-Lamberts	3.426	candela/m^2	cd/m^2
		FORCE and PRESSURE or STRESS		
lbf	poundforce	4.45	newtons	N
lbf/in^2	poundforce per square inch	6.89	kilopascals	kPa

APPROXIMATE CONVERSIONS FROM SI UNITS

Symbol	When You Know	Multiply By	To Find	Symbol
		LENGTH		
mm	millimeters	0.039	inches	in
m	meters	3.28	feet	ft
m	meters	1.09	yards	yd
km	kilometers	0.621	miles	mi
		AREA		
mm^2	square millimeters	0.0016	square inches	in^2
m^2	square meters	10.764	square feet	ft^2
m^2	square meters	1.195	square yards	yd^2
ha	hectares	2.47	acres	ac
km^2	square kilometers	0.386	square miles	mi^2
		VOLUME		
mL	milliliters	0.034	fluid ounces	fl oz
L	liters	0.264	gallons	gal
m^3	cubic meters	35.314	cubic feet	ft^3
m^3	cubic meters	1.307	cubic yards	yd^3
		MASS		
g	grams	0.035	ounces	oz
kg	kilograms	2.202	pounds	lb
Mg (or "t")	megagrams (or "metric ton")	1.103	short tons (2000 lb)	T
		TEMPERATURE (exact degrees)		
°C	Celsius	1.8C+32	Fahrenheit	°F
		ILLUMINATION		
lx	lux	0.0929	foot-candles	fc
cd/m^2	candela/m^2	0.2919	foot-Lamberts	fl
		FORCE and PRESSURE or STRESS		
N	newtons	0.225	poundforce	lbf
kPa	kilopascals	0.145	poundforce per square inch	lbf/in^2

*SI is the symbol for the International System of Units. Appropriate rounding should be made to comply with Section 4 of ASTM E380.
(Revised March 2003)

TABLE OF CONTENTS

LIST OF FIGURES

LIST OF TABLES

CHAPTER 1. INTRODUCTION

INTRODUCTION

Ultra-high performance concrete (UHPC) is an advanced cementitious composite material. When compared to more conventional cement-based concrete materials, UHPC tends to exhibit superior properties such as exceptional durability, increased strength, and long-term stability.(1) This computational investigation focused on developing a series of finite element optimized sections of UHPC pi-girders to effectively utilize the superior mechanical properties of UHPC. In order to fully utilize the superior mechanical properties of the UHPC, it is necessary to perform a thorough analysis to optimize cross-sections for different span lengths. The progress in the finite element (FE) method and the advent of increasingly powerful computers provide an economic way to investigate this complex parameter analysis. The research was performed using the previously calibrated concrete damage plasticity model to represent the elastic and plastic response of the UHPC in the numerical simulation.

OBJECTIVE

It is known that the UHPC demonstrates different behavior from traditional reinforced concrete, particularly in terms of the tensile mechanical response. The objective of this research program is to develop a series of structurally optimized cross sections based on the UHPC pi-girder concept. The developed highway bridge girders facilitate accelerated construction of robust, simple span structures with spans up to 135 feet (42.7 m).

SUMMARY OF APPROACH

The research discussed herein aims at the development of UHPC pi-girder sections for four bridge spans including 85 feet (24.4 m), 95 feet (30.5 m), 105 feet (36.6 m), and 135 feet (42.7 m). Finite element models based on concrete damage plasticity for UHPC have been previously calibrated through the comparisons of five progressively more sophisticated finite element models to full-scale physical tests on flexural and shear response of a UHPC I-girder and the structural response of a 2nd generation pi-girder.(2~4) The same UHPC material properties of the 2nd generation pi-girder are used in this report. As the bridge span increases, the 2nd generation pi-girder section is revised based on the past results and with few geometric parameters to achieve a section with consistent fabrication process and mechanical efficiency. Three major factors were considered in the development of cross-sections for different span: the transverse bending capacity of the deck in the UHPC pi-girder; the global shear and flexural capacity; the deflection under live load. The transverse bending of the deck was investigated by a simplified single girder model of short span. The global flexure and shear capacity of the girder was also analyzed by a single girder model but with different span length. The deflection check was done by analyzing a multiple girder bridge system to include the load distribution among adjacent girders. Finally, analytical comparison of the sections is presented and summarized to facilitate their practical applications.

OUTLINE OF REPORT

This report is divided into six chapters. Chapter 1 introduces the backgrounds and approaches used in this research. Chapter 2 provides a summary of previous researches, discusses the UHPC research and development history of pi-girder. Chapter 3 describes the finite element modeling of the 2nd generation pi-girder and the calibration of the proposed model. Chapter 4 describes the development of 2nd generation pi-girder sections for different span lengths. Chapter 5 summarizes the parametric analysis results and provides guidelines for bridge designers to select appropriate cross-section. Finally, Chapter 6 presents the conclusions and future work of this research program.

CHAPTER 2. BACKGROUND

INTRODUCTION

This chapter provides background information relevant to the focus of the research effort. The chapter first provides a brief introduction of UHPC constituent materials and material properties. The second section of the chapter describes the history on the development of the concept for the UHPC pi-girder cross section.

ULTR-HIGH PERFORMANCE CONCRETE (UHPC)

UHPC is a new generation of fiber-reinforced cementitious composite material. When compared with conventional concrete, UHPC tends to exhibit superior properties such as advanced strength, durability, and long-term stability. It provides new solutions to the pressing highway bridge deterioration and congestion problems in the United States.

UHPC Constituent Materials

The UHPC used in this study is a product marketed by Lafarge under the name Ductal®. It is currently the only product of this type that is widely available in the U.S. in the quantities necessary for large scale infrastructure applications. A typical UHPC composition is provided in Table 1.

The UHPC is composited of Portland cement, fine sand, silica fume, ground quartz, superplasticizer, accelerator and water. As reported in reference (6), the constituent material proportions were determined, in part, based on an optimization of the granular mixture. This method allows for a finely graded and highly homogeneous concrete matrix. Fine sand, generally between 0.006 and 0.024 inch (150 and 600 µm), is dimensionally the largest granular material. The next largest particle is cement with an average diameter of approximately 0.0006 inch (15 µm). Of similar size is the crushed quartz with an average diameter of 0.004 inch (10 µm). The smallest particle, the silica fume, has a diameter small enough to fill the interstitial voids between the cement and the crushed quartz particles. Dimensionally, the largest constituent in the mix is the steel fiber reinforcement. In this study, the fibers had a diameter of 0.008 inch (0.2 mm), a length of 0.5 inch (12.7 mm), and a minimum tensile strength of 377 ksi (2600 MPa). In this study, the fibers were included in the mix at two percent by volume. Given the relative sizes of the sand and the fibers, the steel fibers are able to reinforce the concrete matrix on the micro level. The result is a cementitious composite mixture that exhibits enhanced mechanical and durability properties.

Table 1. Typical UHPC composition.

Material	Amount (kg/m^3 (lb/yd^3))	Percent by Weight
Portland Cement	712 (1,200)	28.5
Fine Sand	1,020 (1,720)	40.8
Silica Fume	231 (390)	9.3
Ground Quartz	211 (355)	8.4
Superplasticizer	30.7 (51.8)	1.2
Accelerator	30.0 (50.5)	1.2
Steel Fibers	156 (263)	6.2
Water	109 (184)	4.4

UHPC material properties

The research program associated with reference (6) addressed the materials properties of the UHPC investigated in this study. A brief summary of the relevant results from the prior study is presented in Table 2. For the present study, the mechanical properties of the UHPC were set at a design compressive strength of 28 ksi (193 MPa), a ductile tensile strength of 1.4-1.6 ksi (9.7-11.0 MPa), an ultimate tensile strain of 0.007-0.01, and Young’s modulus of 7600 ksi (52 GPa). The UHPC mechanical properties may slightly vary depending on the curing methods and specific mixture design.

UHPC stress-strain curve

To effectively used the UHPC material properties, it requires that the stress-strain behavior to be adequately obtained. Previous research (5) has derived a representative stress-strain curve of UHPC when deployed in a prestressed flexural member. This response is shown in Figure 1. Further research has focused on the compressive and tensile mechanical responses as captured from material scale tests.(6,7,8) For the present study, the assumed UHPC uniaxial stress-strain relationship was simplified to Figure 2, reproduced from reference.(2) The tensile stress-strain relationship is elastic-perfect-plastic with an ultimate strain of 0.01 while the compressive-strain relationship is almost linear until the ultimate strength of 28 ksi (193 MPa). However, it is not recommended to utilize the ultimate tensile strain of the UHPC for the design purpose. A conservative value of 0.003 was defined as the criteria for tensile failure of UHPC in this report.

Table 2. Typical UHPC material properties.

Material Characteristic	Average Result
Compressive Strength (ASTM C39; 28-day strength)	28 ksi (193 MPa)
Modulus of Elasticity (ASTM C469; 28-day modulus)	7600 ksi (52 GPa)
Split Cylinder Cracking Strength (ASTM C496)	1.7 ksi (11.7 MPa)
Prism Flexure Cracking Strength (ASTM C1018; 305-mm span; corrected)	1.3 ksi (9.0 MPa)
Mortar Briquette Cracking Strength (AASHTO T132)	1.2 ksi (8.3 MPa)
Direct Tension Cracking Strength (Axial tensile load)	1.4–1.6 ksi (9.7–11.0 MPa)
Prism Flexural Tensile Toughness (ASTM C1018; 305-mm span)	$I_{30} = 53$
Long-Term Creep Coefficient (ASTM C512; 77 MPa sustained load)	0.29
Long-Term Shrinkage (ASTM C157; initial reading after set)	766 microstrain
Total Shrinkage (Embedded vibrating wire gage)	850 microstrain
Coefficient of Thermal Expansion (AASHTO TP60–00)	$15.6 \text{ x}10^{-6}$ mm/mm/ºC
Chloride Ion Penetrability (ASTM C1202; 28-day test)	18 coulombs
Chloride Ion Permeability (AASHTO T259; 12.7-mm depth)	< 0.1 lb/yd^3 (0.06 kg/m^3)
Scaling Resistance (ASTM C672)	No Scaling
Abrasion Resistance (ASTM C944 2x weight; ground surface)	0.006 ounces (0.17 grams) lost
Freeze-Thaw Resistance (ASTM C666A; 600 cycles)	RDM = 96%
Alkali-Silica Reaction (ASTM C1260; tested for 28 days)	Innocuous

1 MPa = 145 psi
1 kg/m^3 = 1.69 lb/yd^3
1 g = 0.035 ounce

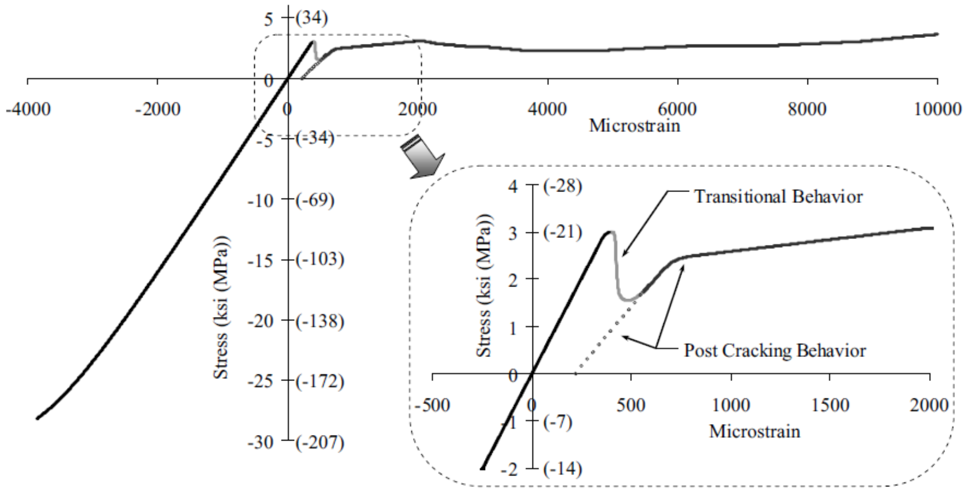

Figure 1. Graph. Derived uniaxial stress-strain behavior of UHPC.

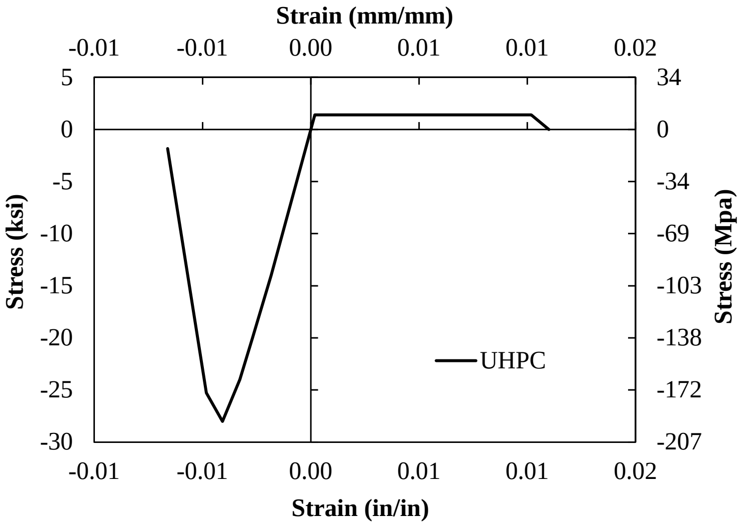

Figure 2. Graph. Assumed UHPC uniaxial stress-strain relationship.

HISTORY OF THE DEVELOPMENT OF UHPC PI-GIRDER

Prototype Pi-Girder Development

The concept of using decked-girder members for bridge applications in transportation and infrastructure is not new. The deck-bulb-tee pre-tensioned concrete girder has been frequently implemented in various parts of the U.S., most notably in the Pacific Northwest. The double-Tee pre-tensioned concrete beam is widely used around the world in parking structures. In New England, governmental and industry partners are beginning to deploy a pre-tensioned double-Tee suitable for short to medium span highway bridges. It is also the case that bridge designs are inherently a function of the mechanical and durability properties of the materials from which the bridge is to be constructed. In the case of reinforced or pre-stressed concrete bridges, these properties and the related design specifications have resulted in bridge component geometries which make efficient use of the material properties.

The development of new materials or the significant modification of the properties of existing materials results in the need for the development of new structural forms. The use of existing geometries for materials with advanced properties, although simple to implement, results in inefficient designs and less cost effective solutions. Advanced material properties bring about the possibility of new design solutions which heretofore may not have been possible. The advanced properties of UHPC provide opportunities for the development of new structural forms focused on addressing any number of important focus areas. Straightforward topics such as creating longer-life bridges through enhanced durability or allowing for the spanning of longer distances with shallower superstructures can be addressed through the use of UHPC. In a systematic sense, UHPC also presents the opportunity to create new structural forms which facilitate accelerated construction and rapid renewal of the highway infrastructure.

The development of a prototype decked girder member which utilized UHPC as the primary structural component was initiated during the early stages of the FHWA UHPC research program, results of which are presented in references (9) and (10). It was evident that UHPC's mechanical and durability properties would allow for beneficial modifications to conventional concrete bridge component solutions as well as development of heretofore not feasible components. Given the exceptional durability properties of UHPC along with its comparatively high compressive and tensile strengths, the development of a decked pre-tensioned girder with slender cross sectional dimensions was an appropriate choice.

The geometric concept for the pi-girder also draws on construction of the Peace Footbridge in Seoul, South Korea.(11) This arch bridge uses post-tensioned construction and the pi-girder cross sectional shape to span 394 feet (120 meters). Although significantly different than conventional highway bridges in the U.S. both in terms of bridge type and loading, this footbridge clearly demonstrated the opportunities that UHPC presents for slender, decked members.

The cross sectional dimensions of the prototype UHPC pi-girder were set through an analytical study completed at the Massachusetts Institute of Technology.(9,10,12,13,14) This research group was selected for this effort as they had completed prior work developing analytical models for the mechanical response of UHPC.(9, 12) The models implemented in the design included one, two, and three dimensional analyses of the predicted response of the girder to the loadings prescribed in the AASHTO LRFD Bridge Design Specification.(15)

Figure 3 presents the prototype pi-girder cross section. The cross section was designed to span between 70 to 100 feet (21.3 and 30.5 m). The girder is 33 inches (0.84 m) deep, 8 feet (2.43 m) wide, and can contain up to 15 pre-stressing strands in each bulb. The integral deck of the girder is 3 inches (76 mm) thick, and the webs range from 2.5 to 3.3 inches (64 to 84 mm) thick. A 6.1 inch (156 mm) deep shear key runs the length of each flange tip to allow for connection of adjacent modular components. Basic properties of the girder include an area of 609 in^2 (0.392 m^2), strong axis moment of inertia of 89,060 in^4 (37.07x10^9 mm^4), and a self-weight of 657 lb/ft (978 kg/m).

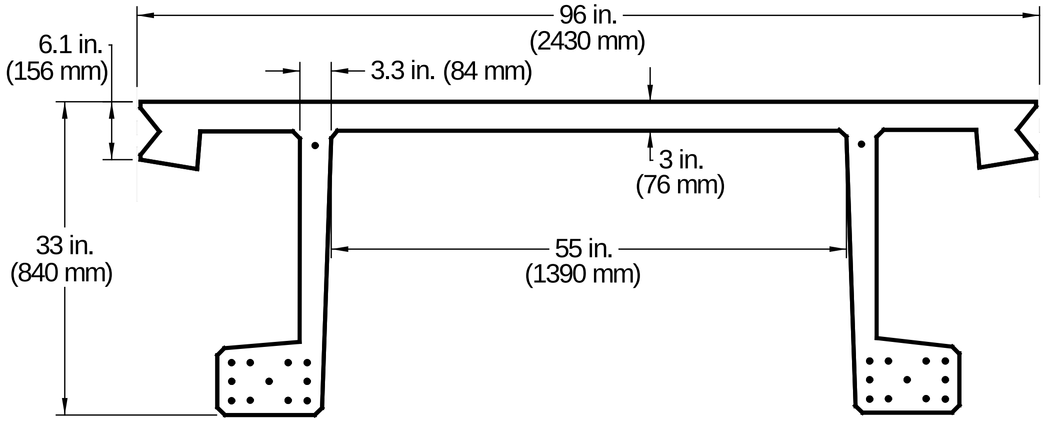

Figure 3. Illustration. Prototype pi-girder cross section and strand pattern.

2nd Generation Pi-Girder Development

An extensive test program was completed which focused on the fabrication and structural performance of the prototype pi-girder. The study demonstrated that the pi-girder concept was feasible; however, minor modifications were necessary in order to simplify girder fabrication and to address some specific structural performance concerns. The modifications which were implemented included: 1) thickening the deck, 2) widening the deck, 3) shifting the legs inward, 4) eliminating the overhang block-outs, 5) thickening the webs, 6) rounding all reentrant corners, and 7) including intermediate diaphragms.

Figure 4 presents the 2nd generation pi-girder cross section. The integral deck of the girder is revised to 4.13 inches (105 mm) thick, and the webs range from 3.2 to 3.5 inches (81 to 89 mm) thick. A 5.25 inch (133 mm) deep diamond-shaped shear key runs the length of each flange tip to allow for connection of adjacent modular components. The internal distance between the bulbs is reduced to 50.5 inch (1.28 m). Basic properties of the girder include an area of 861 in^2 (0.555 m^2), strong axis moment of inertia of 106,000 in^4 ($44x10^9$ mm^4), and a self-weight of 932 lb/ft (1,390 kg/m).

Figure 5 illustrates the overlaid prototype and 2nd generation pi-girder cross sections. Given these modifications to the cross section, basic engineering principles indicate that subjecting the 2nd generation pi-girder to the same battery of structural tests presented in reference (10) would result in increased elastic stiffness and ultimate capacities in primary flexure, primary shear, and transverse flexure.

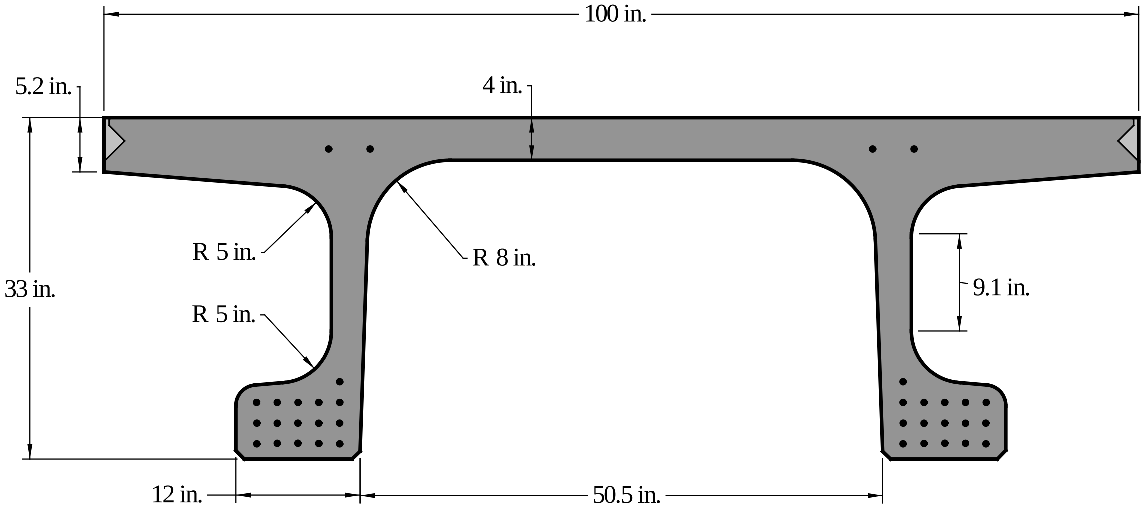

Figure 4. Illustration. 2nd generation pi-girder cross section.

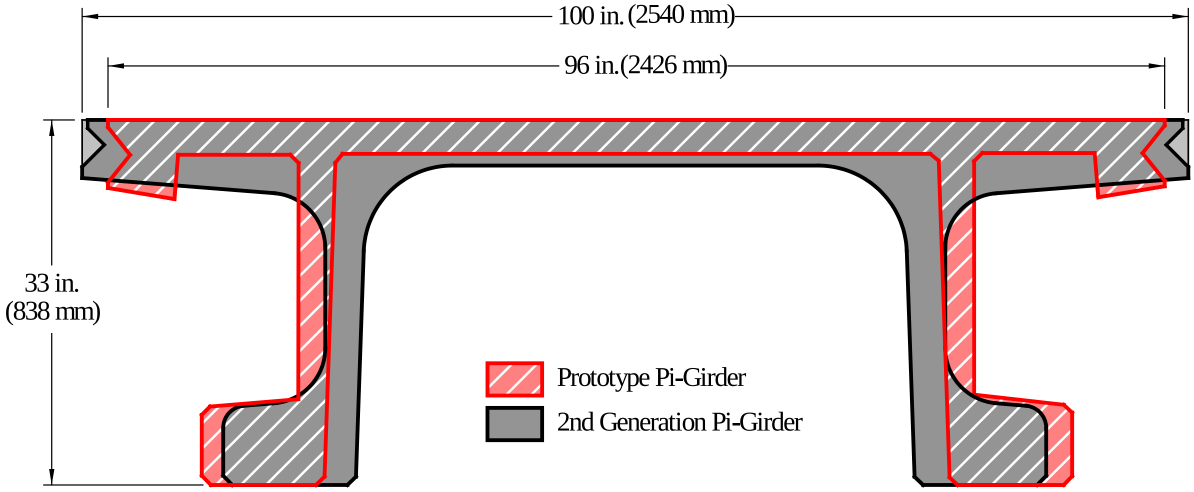

Figure 5. Illustration. Overlaid prototype and 2nd generation pi-girder cross sections.

The structural tests of 2nd generation UHPC pi-girders have been presented in reference (16). The girder is capable of meeting the requirements of the AASHTO LRFD Bridge Design Specifications (15) up to a span length of 87 feet (26.5 m) from the analytical projection. The transverse flexural capacity of the girder is sufficient and the capacity of the longitudinal joint exceeded that of the prefabricated deck.

An initial development of the UHPC pi-girder concept has been completed in Buchanan County, Iowa (17). The Jakway Park Bridge opened to traffic in late 2008. The bridge includes three adjacent 2nd generation UHPC pi-girders, allowing for two lanes traffic.

LOAD AND LOAD FACTORS ---- AASHTO SPECIFICATIONS

The optimized design of pi-girder cross sections is carried out to satisfy both strength and service limit state criteria specified in AASHTO LRFD Bridge Design Specifications(15). This section will define the LRFD design criteria first, then specify the variety of loads and load combinations.

The basic LRFD design equation in the AASHTO LRFD Bridge Specifications that must be satisfied for all limit states is provided in Figure 6.

$$Q \leq R_r$$

$$Q = \Sigma\ \eta_i\, \gamma_i\, Q_i \text{ and } R_r = \phi\, R_n$$

where:

Q – total factored force effect
Q_i – force effect from specified loads
R_n – nominal resistance
R_r – factored resistance
γ_i – load factor
ϕ – resistance factor
η_i – load modifier

Figure 6. Equation. LRFD design criterion

Load Modifier, η

The load modifier, η, takes into account the ductility, redundancy and operational importance of the bridge. η takes on different values for the service limit state (SLS) or the ultimate strength limit state (ULS) and is defined by AASHTO-LRFD

$$\eta = \eta_D \eta_R \eta_I$$

Figure 7. Equation. Load modifier

In Figure 7, the Ductility Factor, η_D =0.95 for ULS (ductile components and connections) and 1.0 for SLS. The Redundancy Factor is, η_R =1.05 for ULS (non-redundant members) and 1.0 for SLS. The last parameter is the Operational Importance Factor, η_I =1.0 for both SLS and ULS (typical bridges). Therefore given these parameters, the load modifier is $\eta = 0.9975 \approx 1$ for both ULS and SLS.

Dead Loads

The dead loads imposed on the pi-girder in this investigation include the self-weight of the UHPC bridge girders (DC_UHPC), the weight of discrete steel reinforcement (DC_SR). Other dead loads such as the weight of pavement wearing surface (DC_WS) and the weight of concrete parapets (DC_CP) do not play significant role in the results and therefore are not included from the analysis.

The self-weight of all structural components can be automatically calculated in the finite element model by multiplying the material density, material volume and gravitational acceleration. The densities of UHPC and steel are assumed to be 160 lb/ft^3 (2565 kg/m^3) and 490 lb/ft^3 (7855 kg/m^3), respectively.

Design Vehicular Live Load

Vehicular live loading on the roadways of bridges, designated HL-93, consists of a combination of the design truck or design tandem and design lane load.

The design lane load consists of a line load of 0.64 klf (9.34 kN/m) uniformly in the longitudinal direction. Transversely, the design lane load is uniformly distributed over a 10-ft (3-m) width. The design lane load (LL_LANE) is equivalent to a uniform pressure of 0.444 psi (441.3 kPa) on a design lane. Multiple Presence Factor, *m*, need to be considered for multiple presence of live load. For 1, 2, and 3 loaded lanes, the value of *m* equals 1.2, 1.00, and 0.85 respectively. The lane load can be partially applied on the deck to achieve the worst loading scenarios for deck or girder bulbs according to the influence line.

Figure 8 specifies the weights and spacing of axles and wheels for the design truck (LL_TRUCK). A dynamic load allowance of 1.33 is considered. The spacing between the two 32-kip (142-kN) axles varied between 14 ft (4.3 m) and 30 ft (9.1 m) to produce extreme force effects.

Design tandem load consist of a pair of 25-kip (111.2-kN) axles spaced 4 ft (1.2 m) apart (LL_TANDEM). The transverse spacing of wheels is taken as 6 ft (1.8 m). A dynamic load allowance of 1.33 is also considered. Generally, the design tandem load is smaller than the design lane load and is unlikely to become the controlling load combination.

The tire contact area of a wheel consisting one or two tires is assumed to be a single rectangle, whose width is 20 in (508 mm) and whose length is 10 in (254 mm). The tire pressure is assumed to be uniformly distributed over the contact area. The design load is always an axle load and single wheel loads are not considered according to AASHTO specifications.

The total design truck load is 8 kip + 32 kip × 2 = 72 kip (320 kN). Its front tire pressure is 8 kip/(20 in × 10 in × 2) = 20 psi (138 kPa) and its rear tire pressure is 32 kip/ /(20 in × 10 in × 2) = 80 psi (552 kPa). The total design tandem load is 25 kip × 2 = 50 kip (222.4 kN). Its tire pressure is 25 kip/(20 in × 10 in × 2) = 62.5 psi (431 kPa). The design wheel load has to be multiplied by the dynamic impact factor, $\delta = 1.33$, in calculating factored loads.

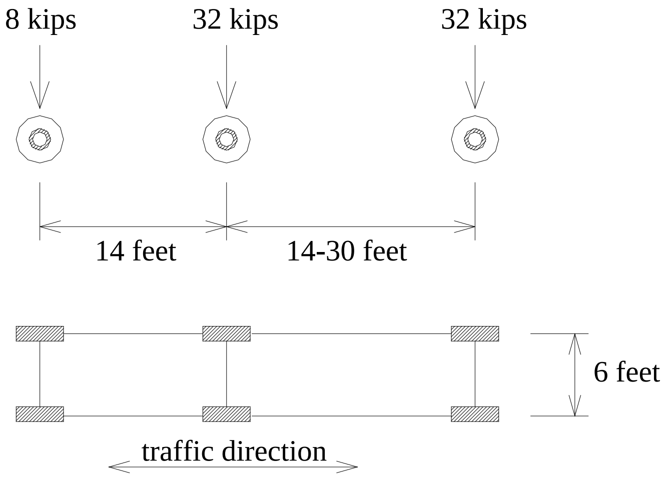

Figure 8. Illustration. Design Truck Load Specifications (from AASHTO).

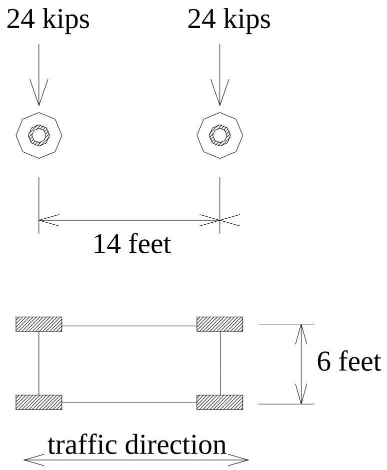

Figure 9. Illustration. Design Tandem Load Specifications (from AASHTO).

Load Factors

A UHPC girder bridge needs to satisfy the equation in Figure 6 for the two combinations of factored extreme force effects: SERVICE III and STRENGTH I. Loading combination relating to vehicle collision needs to check EXTREME EVENT II.

SERVICE III – load combination for longitudinal analysis relating to tension in prestressed concrete superstructures with the objective of crack control.(15)

$$Q_{Service\_III} = DC + DW + 0.8LL = DC\_UHPC + DC\_CP + DC\_SR + DW + 0.8 \times (LL\_LANE + IM * LL\_TRUCK \text{ or } LL\_TANDEM) \times m$$

where:
DC – Dead load of structural components and non-structural attachments
DW – Dead load of wearing surface and utilities
LL – Vehicular Live Load

Figure 10. Equation. Service III load combination

STRENGTH I - basic load combination relating to the normal vehicular use of the bridge without wind. (15)

This limit state represents the maximum possible load that the structure is designed to sustain. The suggested load factors are:

$$Q_{Strengh\_I} = 1.25\ DC + 1.5DW + 1.75LL = 1.25 \times (DC\_UHPC + DC\_CP + DC\_SR) + 1.5 \times DW + 1.75 \times (\ LL\_LANE + IM\ {*}LL\_TRUCK\ or\ LL\_TANDEM) \times m$$

Figure 11. Equation. Strength I load combination

Table 3. Load combination as per AASHTO-LRFD specifications.

Loads	**DC**	**DW**	**LL_LANE**	**LL_TANDEM**	**LL_TRUCK**	
					front tire	rear tire
Service III	1.00	1.00	0.80	0.80	0.80	0.80
Strength I	1.25	1. 50	1.75	1.75	1.75	1.75
Extreme II	1.25-0.9	1.5-0.65	0.5	0.5	0.5	0.5
Dynamic Load Allowance	-	-	-	1.33 (1.75 for deck joint study)		
Multiple Presence Factor	-	-	1.20 / 1 lane 1.00 / 2 lanes 0.85 / 3 lanes			
Nominal Loads (psi (MPa))	310 (4970)	0.174 (1.2)	0.444 (3.1)	62.5 (431)	20.0 (138)	80.0 (552)

EXTREME EVENT II – load combination relating to collision by vehicles.

The limit state is determined by checking the stress and strain in the deck near the concrete parapet when the upper and lower limit of γ_p are applied to dead loads and other live loads. The suggested load factors are:

$$Q_{Extreme\_II} = \gamma_p\, DC + \gamma_p\, DW + 0.5LL = \gamma_p \times (DC\_UHPC + DC\_CP + DC\_SR) + \gamma_p \times DW + 0.5 \times (\, LL\_LANE + IM * LL\_TRUCK \text{ or } LL\_TANDEM) \times m + F_L + F_t$$

Figure 12. Equation. Extreme event II load combination

CHAPTER 3. FINITE ELEMENT MODELLING OF UHPC PI-GIRDER

INTRODUCTION

Even though the capacity of sections can be approximated through simplified analysis, the finite element model can provide a more accurate and comprehensive prediction considering calibrated material model covering both elastic and plastic response, three dimensional deformation, realistic component geometry, and structural interactions. This chapter provides a comprehensive study on the analysis of UHPC pi-girders using finite element method (FEM). The first part details the development of the finite element model used in the research. The second part describes how the developed model in the first part was calibrated using experimental data.

FINITE ELEMENT MODELING OF PI-SECTIONS OF UHPC GIRDERS

Finite Element Method

The finite element analysis (FEA) or finite element method (FEM) originated from the need to solve complex structural analysis problems in aeronautical and civil engineering. The FEM is a numerical technique for finding approximate solutions of partial differential equations (PDE) through a discretization of a complex problem domain into small simple parts (elements) and an assemblage of simple element equations in each element into a set of global finite element equations. The global finite element equations govern the whole domain by applying nodal continuity conditions and boundary conditions. This method eliminates the partial differential equations by transforming them into a set of approximate ordinary differential equations (ODE) which can be solved by standard numerical techniques for simultaneous linear algebraic equations. General steps of FEA includes: (1) mesh, to discretize the domain into elements; (2) build local stiffness matrix and assemble global stiffness matrix and set up system equations; (3) apply boundary conditions to remove columns and rows in the system equations; (4) solve the system equation to determine the values of unconfined degrees of freedoms; (5) solve for strain and stress using the results from step (4).

With the development of modern computer science and technologies, commercial FEM software now allows detailed visualization of structures, estimation of the distribution of stresses and displacements; identification of critical components; and the facilitation of the completion of parametric studies. FEM allows entire designs to be constructed, refined, and optimized before the final product is fabricated and standardized. The introduction of FEM can substantially decrease the time to take products from concept to production. At the same time FEM offers benefits including increased accuracy, enhanced design, and better insight into critical design parameters, virtual prototyping, fewer hardware prototypes, less physical testing, and a faster yet less expensive design cycle.

Abaqus

ABAQUS was initially developed by Hibbitt, Karlsson & Sorenson Inc. of Rhode Island, a company founded in 1978 and acquired by Dassault Systèmes Simulia in 2005.(18) The package is popular with academic and research institutions because it has an extensive range of material models and strong capabilities in nonlinear problems. The ABAQUS suite consists of three products: ABAQUS/Standard, ABAQUS/Explicit, and ABAQUS/CAE. ABAQUS/Standard is a general-purpose solver using a traditional implicit integration scheme to solve finite element analysis. ABAQUS/Explicit uses an explicit integration scheme to solve highly nonlinear transient dynamic and quasi-static analysis. ABAQUS/CAE provides an interactive preprocessing and postprocessing environment. In this research program, ABAQUS/CAE was used to create finite element models and the associated input files for ABAQUS/Standard, and to view the results obtained from ABAQUS/Standard solver.

Modeling of Concrete

The concrete damage plasticity (CDP) model was used in this study to model the behavior of concrete. CDP assumes scalar (isotropic) damage elasticity in combination with isotropic tensile and compressive plasticity to represent the inelastic behavior of concrete. It can handle concrete structures subjected to arbitrary loading conditions including cyclic and/or dynamic loading. It also allows stiffness recovery effects during cyclic load reversals. This model assumes non-associated potential plastic flow. Formation of tensile micro-cracks is represented macroscopically with a softening stress-strain relationship and similarly its compressive plastic response is typically represented by stress hardening followed by strain softening beyond the ultimate compressive stress. If needed, damage variables can be included in a CDP model to predict damage and stiffness recovery during cyclic load reversals. References (19) through (22) provide theoretical background for the model to be used herein.

The CDP model assumes two failure mechanisms, namely, tensile cracking and compressive crushing of the concrete material. It also allows stiffness recovery effects during cyclic load reversals. This model assumes non-associated potential plastic flow. Formation of tensile micro-cracks is represented macroscopically with a softening stress-strain relationship and similarly its compressive plastic response is typically represented by stress hardening followed by strain softening beyond the ultimate compressive stress. Schematic yield surface in three-dimensional stress space can be found on page 41 of reference (19). The yield surface can expand or shrink from the initial and subsequent yield surfaces following the hardening or softening rule.

Density, elastic modulus, and compression hardening can be obtained from experimental test data. However, defining tension stiffening is more difficult and is critical to accurately predicting the response of a modeled structural member. There are three ways: post-failure stress-strain relationship, post-failure stress-displacement relationship, and post-failure stress-fracture energy relationship. The post-failure stress-displacement relationship of a material can be converted into its post-failure stress-fracture energy relationship because the area under a stress-displacement response is fracture energy, G_f. The five additional parameters required to fully describe a CDP model include dilation angle in degrees, flow potential eccentricity, ratio of initial equibiaxial compressive yield stress to initial uniaxial compressive yield stress, ratio of the second stress invariant on the tensile meridian to that on the compressive meridian, and a viscosity parameter that defines visco-plastic regularization. These default values are 15^{o}, 0.1, 1.16, 2/3, and 0.0, respectively.

Table 4 provides the CDP parameters for the UHPC with 2% fiber reinforcement by volume with three tension stiffening definitions. The parameters were calibrated in the 2nd generation pi-girders as presented in reference (2). The CDP parameters are used in this investigation. In order to capture the three-dimensional behavior of the UHPC pi-girder, an 8-node linear brick element with reduced integration (C3D8R) was used for concrete elements.

Table 4. Material parameters for the CDP model of the UHPC used in the pi-girder tests.

Properties	Parameters and Values	
Concrete weight		
	Density, lb/ft^3 (kg/m^3)	160 (2565)
Concrete elasticity		
	E, ksi (GPa)	7650 (53)
	ν	0.18
Concrete compression hardening		
	Compressive stress ksi (MPa)	Plastic strain (-)
	14 (97)	0.0000000
	16 (110)	0.0000284
	20 (138)	0.0000720
	24 (166)	0.0001410
	28 (193)	0.0004140
Concrete tension stiffening (strain-stress)		
	Tensile stress ksi (MPa)	Plastic strain (+)
	1.4 (9.7)	0.000
	1.4 (9.7)	0.010
	0.0 (0.0)	0.011
Concrete tension stiffening (strain-fracture energy)		
	Tensile stress, ksi (MPa)	Fracture energy, lb/inch (N/m)
	1.4 (9.7)	500 (87559)

Modeling of Strands

The stress-strain curve for 270 ksi (1862 MPa) strand is shown in Figure 13. In the pi-girder, all strands in the bulbs and in the deck were prestressed to magnitudes of 183.8 ksi (1267 MPa) in the longitudinal direction. The pre-stress was applied in the form of initial stress in the strand elements.

The prestressing strand commonly deployed in bridge girders consists of seven high-stress wires. In the finite element modeling, it is not necessary to model each individual wire. In order to reduce mesh density in the modeled strands, a square of equivalent steel area 0.22 in^2 (142 mm^2) replaces the original wire bundle (See Figure 14). The interaction between the concrete and discrete steel reinforcement such as strands was achieved by embedding the reinforcements in the concrete, assuming no bond-slip between strands and neighboring UHPC.

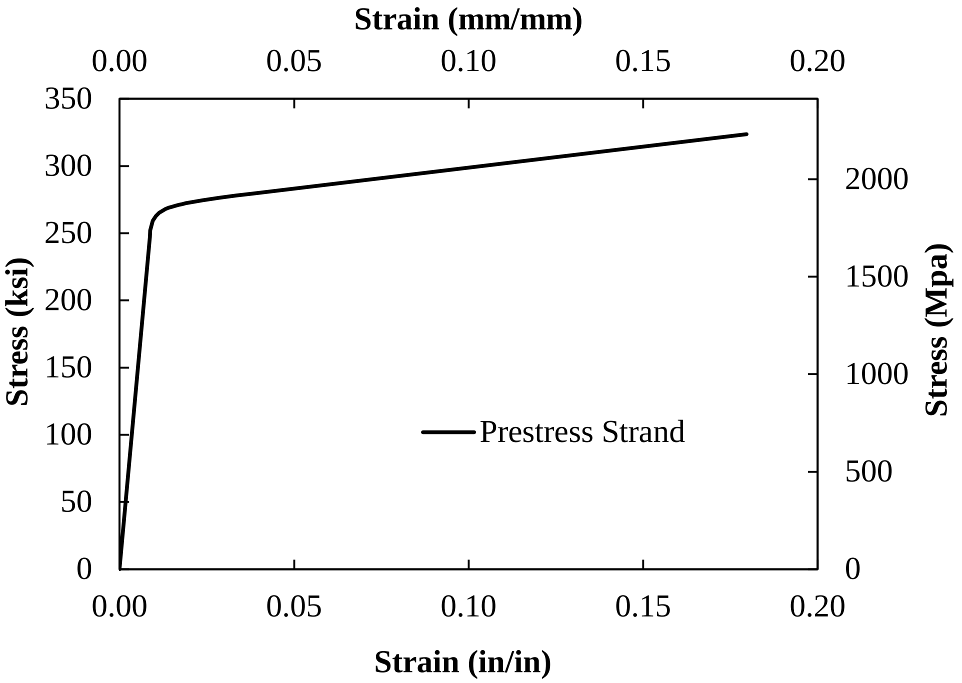

Figure 13. Graph. Uniaxial stress-strain relationships of prestressing strands.

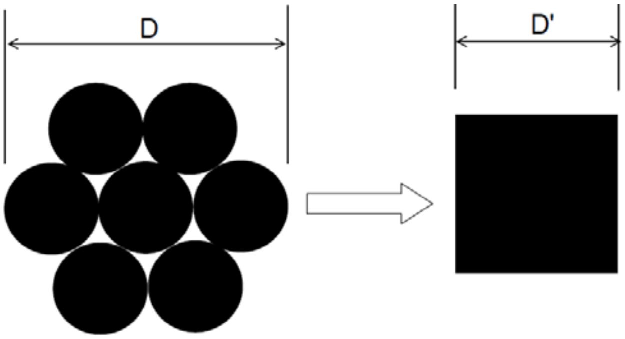

Figure 14. Illustration. Equivalent shape of prestressing strands

Modeling of Diaphragm

The structural behavior of pi-girders can be greatly enhanced by installing intermediate diaphragms. The effect of diaphragm has been demonstrated in the pi-girder and pi-girder-with-joint tests in reference (2). Figure 15 and Figure 16 show the details of the diaphragms. Figure 15 shows the two different diaphragms configurations with one, which is relatively long, designed for the space between legs of an individual girder and the other, which is relatively short, designed to span the transverse distance between the bulbs of two adjacent girders. Figure 16 shows the details of the end plates welded onto the end of the steel tubes that comprise the length of the diaphragms. It is found that the short diaphragm was significantly weakened by the milled end plates prior to the installation of these diaphragms into the space between the girder legs. However, the axial mechanical property of the short diaphragm can be estimated from the long diaphragm by excluding the additional deformation of the 25 inch (635 mm) longer steel tube in the long diaphragm. Table 5 lists the properties of the nonlinear springs which replicate both short and long diaphragms. Figure 17 plots the assumed nonlinear spring responses. The effect of diaphragm stiffness is investigated in the 80-ft span bridge model in the next chapter.

In practice, the end diaphragm may be constructed in the field from field-cast concrete, limiting the stress concentration on the bridge ends and enhancing the girder's stiffness in the transition between a bridge and a bridge abutment. Therefore this type of the end diaphragm needs to be investigated for its effect on both local and global response of the girders.

The diaphragms have been modeled as nonlinear springs bracing the girder legs. To prevent the stress concentration at the anchorage of the spring, the two ends of the spring were anchored to two rigid plates and one side of the plates was tied to the surface of UHPC girder, assuming no relative displacement between the rigid plates and UHPC girder.

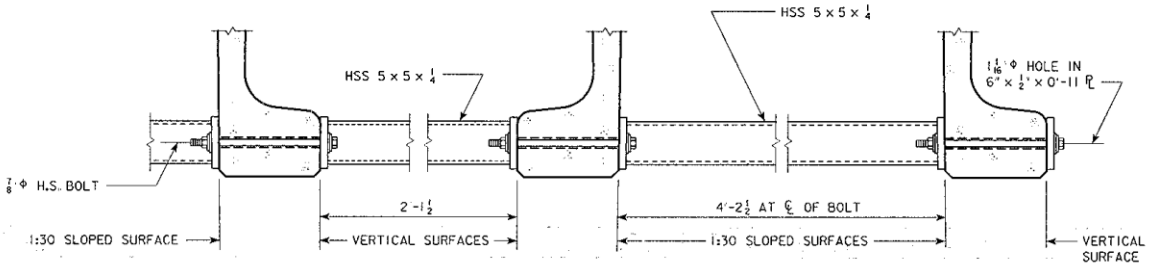

Figure 15. Illustration. Elevation view of diaphragms.

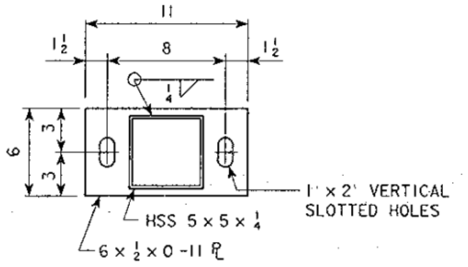

Figure 16. Illustration. End view of diaphragm end plate.

Table 5. Properties of the nonlinear springs which replicate the diaphragms in a pi-girder.

Axial Force, kip (kN)	Axial Elongation, inch (mm)	
	Short diaphragm	Long diaphragm
-10 (-44)	-0.0115 (-0.292)	-0.0095 (-0.241)
0 (0)	0.0000 (0.000)	0.0000 (0.000)
5 (22)	0.0036 (0.091)	0.0046 (0.117)
10 (44)	0.0075 (0.190)	0.0095 (0.241)
15 (67)	0.0124 (0.315)	0.0154 (0.391)
20 (89)	0.0212 (0.538)	0.0252 (0.640)
25 (111)	0.0391 (0.993)	0.0441 (1.120)
30 (133)	0.0740 (1.879)	0.0800 (2.032)
35 (156)	0.1230 (3.124)	0.1300 (3.302)
40 (178)	0.1920 (4.876)	0.2000 (5.080)
50 (222)	0.3900 (9.905)	0.4000 (10.160)

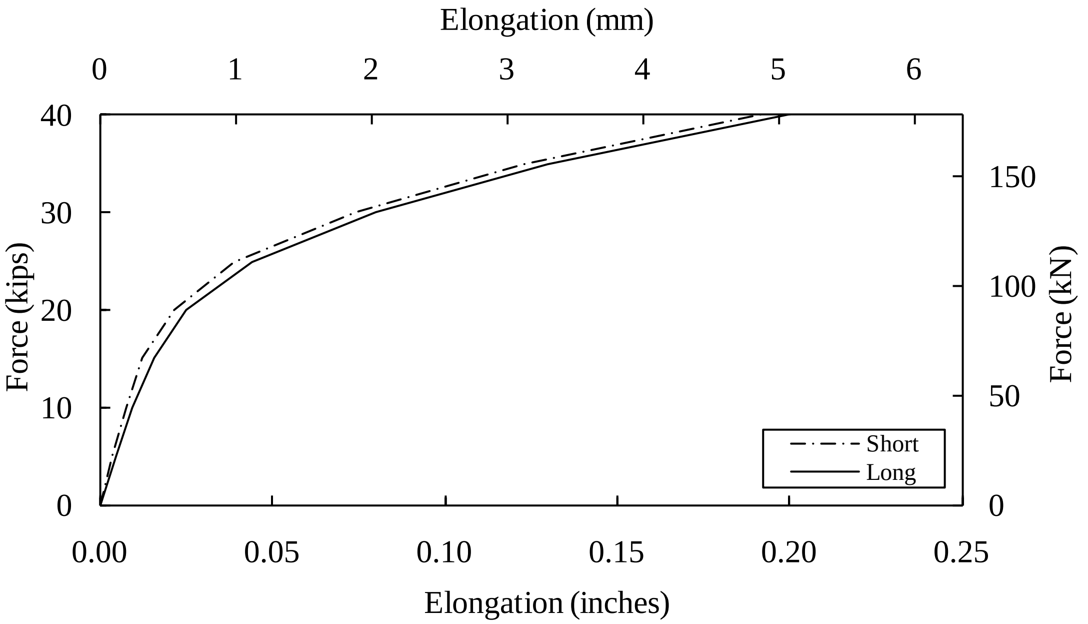

Figure 17. Graph. Behaviors of assumed nonlinear springs for both short and long diaphragms.

Modeling of Other Elements

The support condition of the girder has significant influence on the behavior of the girder. It is therefore necessary to appropriately model the boundary conditions. This research focuses on the development of cross-sections for simply support girders with different spans. To avoid stress concentrations near the supports, a very stiff bottom pad was created and one surface of the pad was tied to the surface of the pi-girder. The bottom pad was then connected to the "ground" by springs at one point. The purpose of this is to allow the free rotation at the support. The stiffness of the vertical spring (in y-direction) was artificially assigned with a high stiffness while the stiffness in the transverse direction (x-direction) was assigned with a very load number to allow for the spread of the leg, as shown in Figure 18. The displacement in the longitudinal direction (z-direction) was restrained on one end of the girder. There is no longitudinal restraint on the other end. In this way, a simply supported boundary condition was simulated.

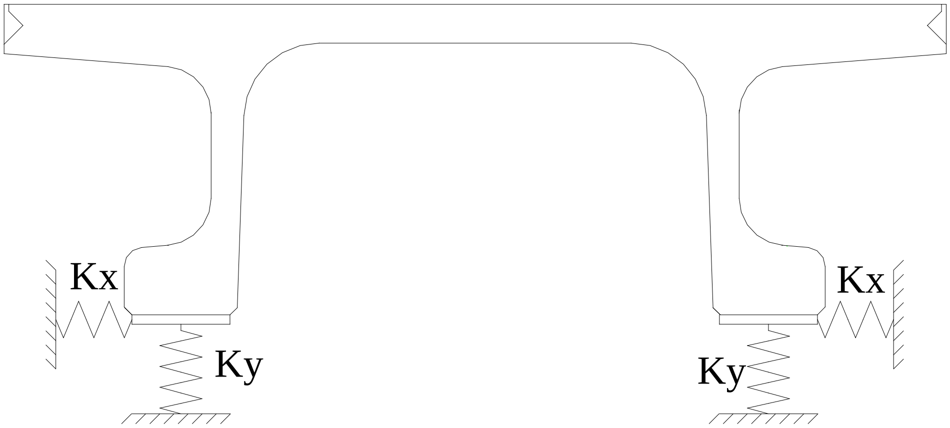

Figure 18. Illustration. Boundary Conditions in the Finite Element Model.

In the multi-girder system, the connection between girders plays an important role in distributing the load transversely among girders. For simplicity, the interface between girders was assumed to be fully connected in this research, i.e. no slip was assumed. This was simulated by applying tie constraint at the interface such that all degrees of freedom for all nodes at the interface were coupled.

In the development of the optimized cross-section, the controlling factor is the lane load and the wheel loads. In this research, the load was applied as a pressure on a surface which can be moved to any location on the model. This makes it is easier to change the load location for different cases. The surface where the load was applied was fully tied to the girder using the tie constraint.

In a finite element model, multiple load processes or multiple load combinations can be achieved by grouping sequential loading steps. In the problem investigated here, two loading steps were proposed to mimic the construction sequence of the bridge and accommodate different load factors.

Initially, the discrete steel strands were embedded in the concrete. The girder bulbs were braced by the diaphragms. The girders were tied to base plates and base plates were restrained by springs in all x and y directions and fixed in z direction. The loading surfaces were tied to the deck top surface with no load applied on them and the interfaces on adjacent girders were tied.

The prestressing force was created in the girders by assigning an initial stress to the strands, after which the prefabricated beam comes to an equilibrium condition. In order to account for the inelastic losses that inherently occur in a prestressed concrete beam, the initial stress in the strands was set at 183.8 ksi (1267 MPa), which is equivalent to 68 percent of the nominal ultimate strength of the strands. This includes a lump-sum prestress loss that accounts for losses due to creep, shrinkage, etc. After this initial step, the diaphragms were activated and the load was applied.

CALIBRATION OF FINITE ELEMENT MODELS

A 25-foot (7.62 m) long UHPC pi-girder was tested in the lab (23) and a finite element model using the techniques described earlier was built and analyzed in reference (2). The proposed model was calibrated by comparing the experimental results with the results from finite element analysis. A summary of the results of that study are presented below.

Experimental Work

A full scale structural test was conducted in the TFHRC structural testing laboratory to investigate the behavior of the 2nd generation pi-girder. The 2nd generation cross section is shown in Figure 19. The girder is 33 inches (0.84 m) deep, 8.33 feet (2.54 m) wide, and can contain up to 16 prestressing strands in each bulb. The integral deck of the girder is 4.13 inches (105 mm) thick, and the webs range from 3.2 to 3.5 inches (81 to 89 mm) thick. A 5.25 inch (133 mm) deep shear key runs the length of each flange tip to allow for connection of the modular components. Basic properties of the girder include an area of 861 in^2 (0.555 m^2), strong axis moment of inertia of approximately 106,000 in^4 (44x109 mm^4), and a self-weight of 932 lb/ft (1,390 kg/m). Two diaphragms were included in the test girder to assist in maintaining the integrity of the cross section during erection and under structural loading. The diaphragms were each located 6 feet (1.83m) from midspan. The girder was prestressed through the use of 0.6 inch (15.2mm) diameter, 270 ksi (1860 MPa) low-relaxation prestressing strands. The girder had 22 strands with nine in each of the two bulbs and two in the deck above each web. The strands in the bulb were all stressed to 42.5 kips (189 kN). The strands in the deck were each pulled to 5 kips (22 kN). The test step scheme and actual setup is shown in Figure 20 and Figure 21. The girder was loaded to failure under gradually increased static loading.

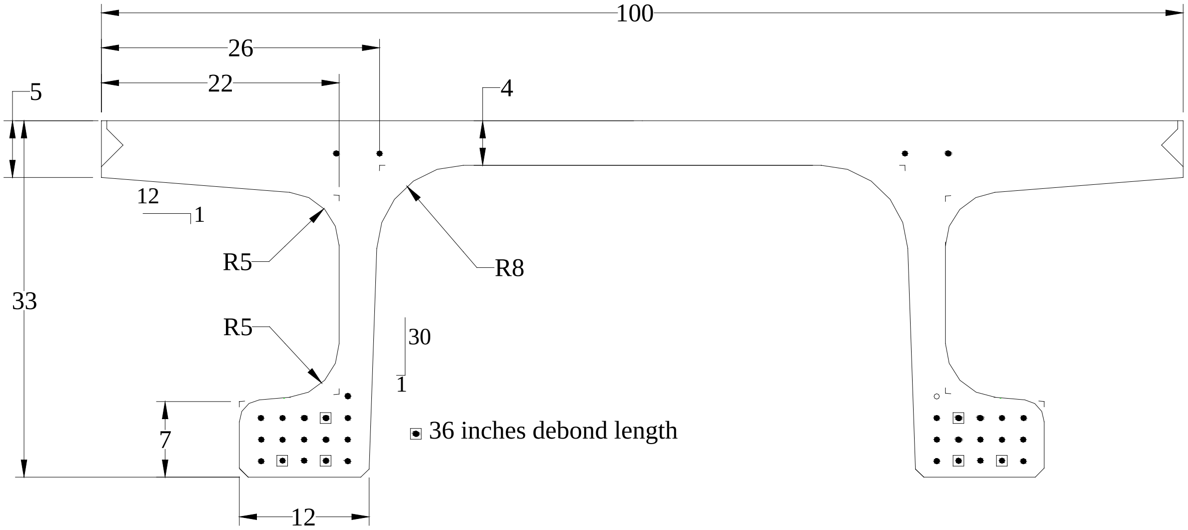

Figure 19. Illustration. Girder cross section and strand pattern.

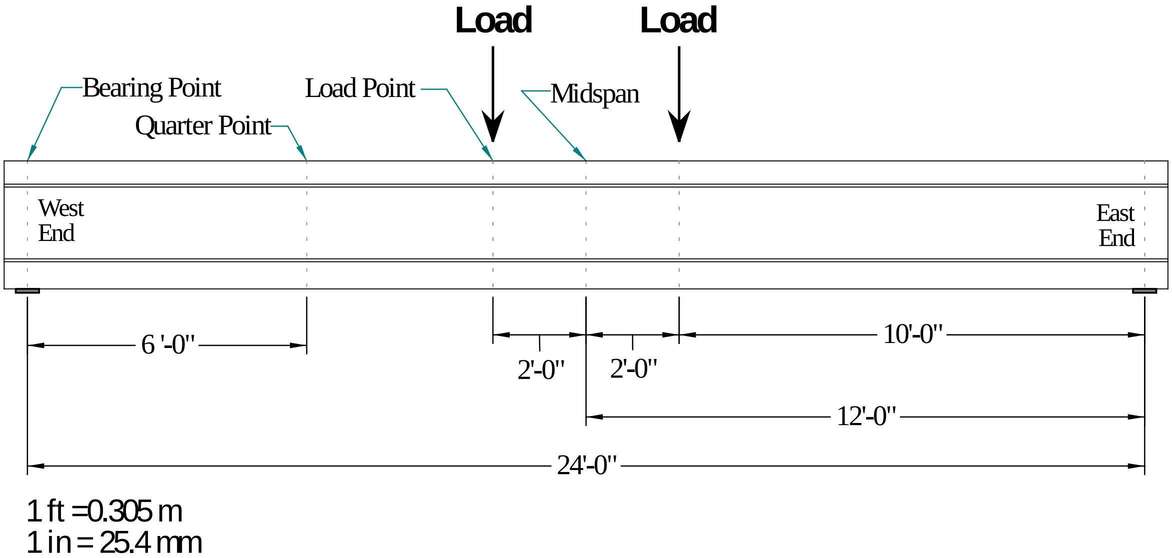

Figure 20. Illustration. Loading Setup.

Figure 21. Photo. Test Setup in the Lab.

Finite Element Analysis Results

Finite element model that simulates the behavior of the girder under test was built using previously described techniques. Experimental results and results from FEA are compared in this section. Figure 22 compares the FEA and experimentally observed vertical deflections of the bulbs at the mid-span. The bulb deflection at mid-span is representative of the global longitudinal flexure of the girder. It can be seen that the experiment results and FEA results agree well and the stiffening effect was successfully captured. The lateral spreading of the bulb under load may lead to the apparent stiffening of the girder response. The difference between the two may be contributed that fact that the non-linear behavior of the bottom pad at the support was not completely accurate. Figure 23 and Figure 24 compared the spreading of the bulb at the mid-span and at the supports, respectively. Again, the experimentally observed results and the FEA results match quite well.

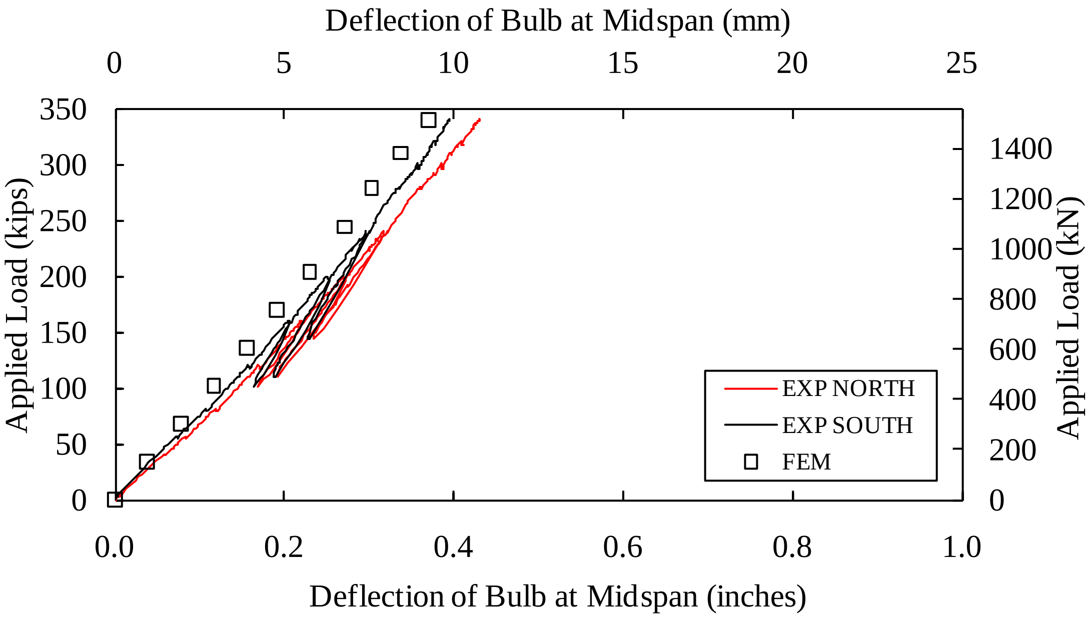

Figure 22. Graph. Comparison of Vertical Bulb Deflection at Midspan.

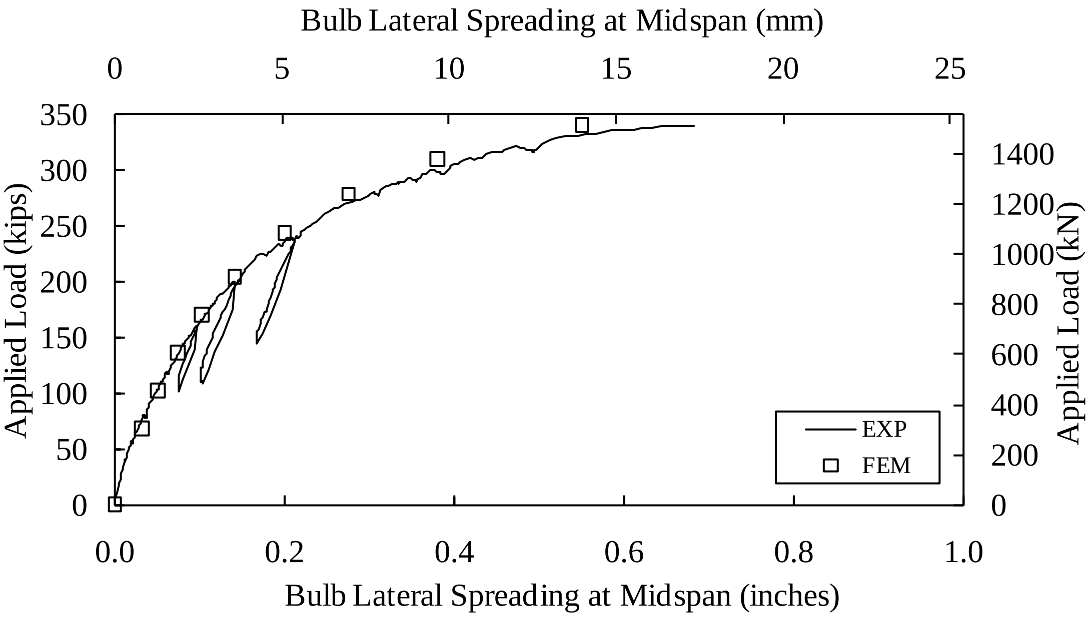

Figure 23. Graph. Comparison of Bulb Spreading at Midspan.

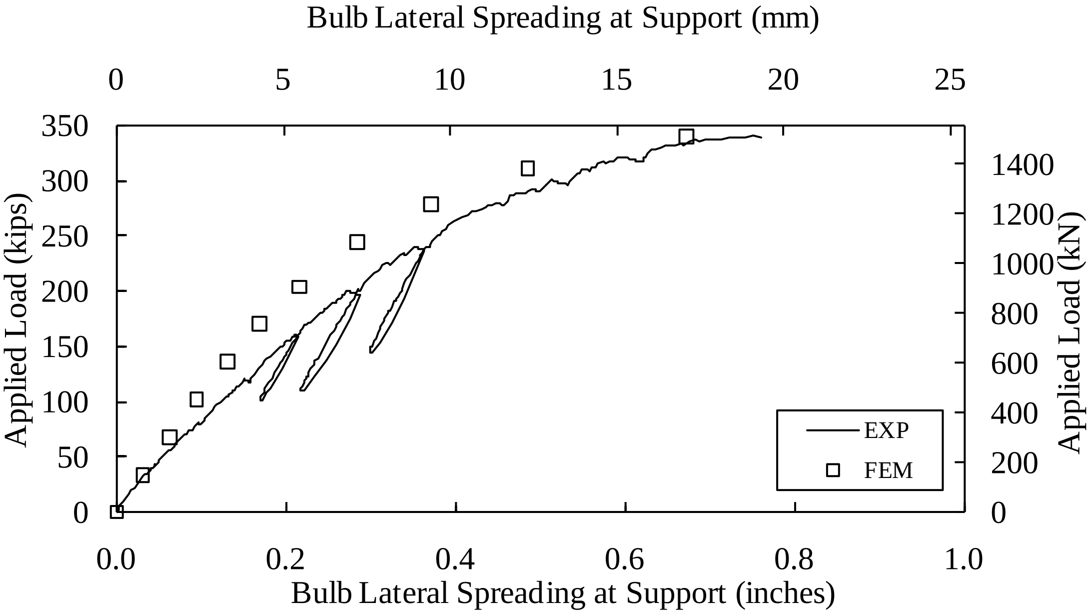

Figure 24. Graph. Comparison of Bulb Spreading at Support.

The proposed FEA model was able to not only predict the deflection but capture the strain response. Figure 25 and Figure 26 showed the difference between experimental and FEA results for the longitudinal strain at the bottom of the bulb and above the web at midspan. Good agreements were achieved between experimental results and numerical simulation. As reported in reference (2), discrepancies were observed in the transverse strain at midspan mid-deck when the applied load was above 60 kips (267 kN). This likely resulted from the cracking of the deck at the gauge location where the gauge reading is higher than the FEA prediction. The FEA model was not intended to capture this local behavior.

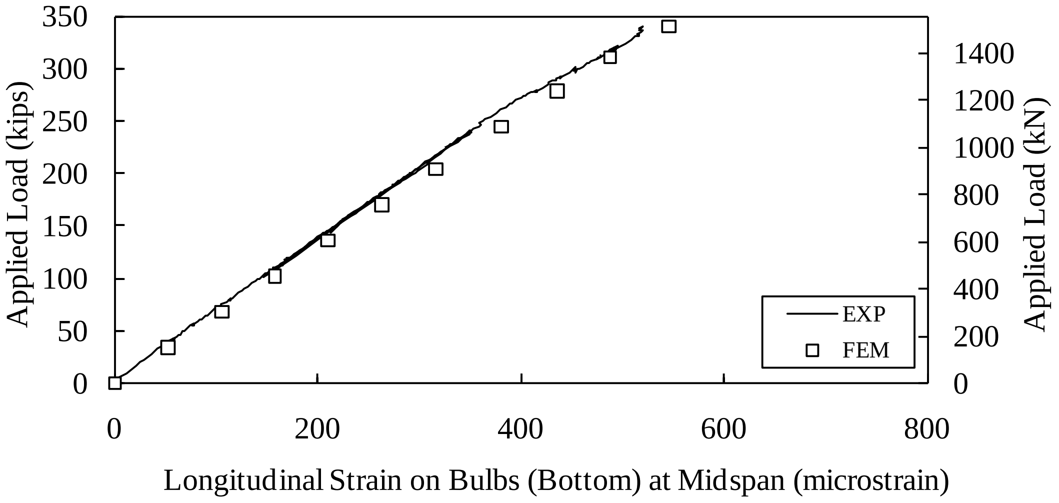

Figure 25. Graph. Comparison of Strain at Bulb bottom at Midspan.

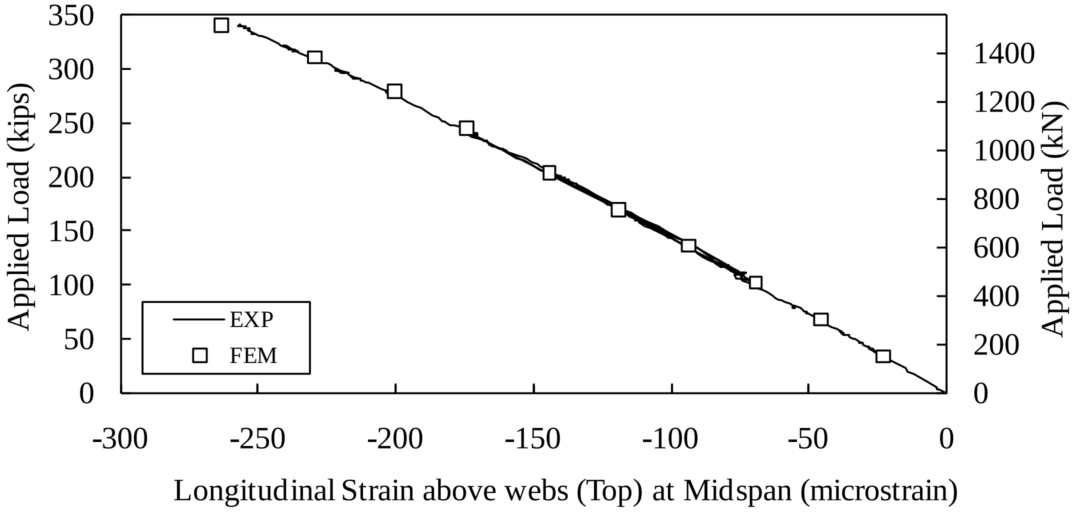

Figure 26. Graph. Comparison of Strain above Webs at Midspan.

SUMMARY

This chapter describes the techniques used in the modeling of pi-girder and the proposed FEA model was calibrated through comparison between the experimentally observed and numerical results. The comparison showed that the proposed FEA model can effectively capture the global deflection and strain distribution. The FEA model can therefore be extended for the development of optimal cross sections for different spans as will be described in the next chapter.

CHAPTER 4. DEVELOPMENT OF UHPC PI-SECTIONS FOR DIFFERENT SPANS

INTRODUCTION

The finite element model was calibrated by comparing the numerical results and experimental measurements in CHAPTER 3. This makes it possible to develop a series of cross sections for different spans that make full use of the superior mechanical properties of UHPC. This chapter focuses on how the cross section was developed for different spans. There are many factors that can affect the capacity and behavior of the girder. In this research, major parameters include the girder height, bulb size, deck thickness, and layouts of pre-stress strands. As mentioned before, three factors need to be considered in the development of optimal cross section: transverse bending capacity of the deck; global flexural and shear capacity of the girder; and the global deflection under live load. The purpose of this chapter is to find the optimal value for these parameters for a certain span or find the maximum span (under simply supported condition) at which the cross section can meet the requirements.

DECK THICKNESS ANALYSIS

This section focuses on the analysis of the deck thickness in pi-sections. The motivation to investigate the deck thickness comes from two considerations. Due to the high tensile strength of the UHPC, the thickness of the deck in the pi-section can be thinner than the deck thickness of a traditional concrete bridge deck. But when the deck is too thin, the section may fail in the form of transverse bending under wheel load. The goal here becomes to find a thickness that prevents transverse bending failure of the pi-section. The analysis considers both AASHTO LRFD-defined wheel loads as well as more severe wheel loadings that may occur in practice.

Factors Considered in the Finite Element Models

The behavior of the deck in the pi-girder sections can be considered as a two-way slab. This adds complexity to the investigation as changes in one direction may affect the behavior in the other direction, especially when the effect of diaphragm is considered. A closer investigation showed that when the span is short, the transverse bending capacity controls the behavior of the pi-girder. This is because the web and bulb in the pi-section stiffen the section in the longitudinal direction as compared with the transverse direction. The longitudinal flexural and shear response of the girder is heavily influenced by the span length, while the transverse response is not. In order to investigate the transverse bending capacity, it is important that other failure modes such as longitudinal flexural failure and shear failure be suppressed. Accordingly, a short span model is needed to suppress the longitudinal failure and investigate the transverse bending capacity. In this portion of the research the span length used in the deck thickness analysis is 15 feet (4.57m), which is close to diaphragm spacing used in the Jakway Park Bridge.(17)

Another factor that affects the transverse bending capacity is the stiffness of the diaphragm and the spacing between diaphragms. As described in Chapter 2, the diaphragm was modeled as a non-linear spring using a connector element. The spring parameters were determined from experimental data. The diaphragm with stiffness properties from experimental measurement is referred to as the regular diaphragm for the rest of the report. To investigate the effect of the diaphragm stiffness, a very soft diaphragm was modeled using a stiffness close to zero ($1X10^{-8}$ lb/in. ($1.75X10^{-6}$N/m)) and a very stiff diaphragm was modeled using a high stiffness value ($1X10^{15}$ lb/in. ($1.75X10^{17}$ N/m)).

The load pattern on the deck has an important effect on the behavior of the girder. The wheel load on a bridge deck is a pressure over a contact area. As mentioned before, the contact area of a wheel consisting of a pair of tires is assumed to be a single rectangle with 20 inches (508 mm) in the transverse direction of the girder and 10 inches (245 mm) in the longitudinal direction. The distributed pressure over the area is assumed to be uniform. Since the span of the model is only 15 feet (4.57m), there can only be one wheel load applied in the longitudinal direction (i.e., in the traffic direction) on the model. Considering the multiple lanes that may be present on a bridge, it is possible that two trucks may pass through the bridge side by side. Therefore, the wheel load in this section was modeled as two wheel patches adjacent to each other. This is unrealistic as the wheels of two trucks could not be touching; however, this assumption is conservative. The wheel patches were placed at the mid-span in the longitudinal direction as it creates the worst scenario for a simply supported boundary condition. This simulates the condition when the wheels are at the middle point between supports or diaphragms. In the transverse direction, the load patches were placed symmetric about the center of the deck to create maximum transverse bending stress in the deck. The factor for multi-lane presence was not considered in the model as the model only has single girder and the deck width is less than one standard traffic lane (12 feet (3.66m)).

Finite Element Model for Deck Thickness Analysis

Abaqus/Standard version 6.11 was used to perform the analysis. Figure 27 depicts the three-dimensional pi-girder model for deck thickness analysis. As mentioned before, the pi-girder was supported on four steel plates which were modeled in 3D continuum shell element SC8R. The steel plates were pinned in the longitudinal direction in one end. The bottom plates were supported by springs with high-stiffness in Y direction to simulate the support in vertical direction and by soft springs in X direction to prevent rigid body movement in the X direction while allowing for free spreading and rotation of the legs. This simulates the simply supported boundary condition. Since the width of the deck is only 100 inches (254 mm), less than the width of a design lane, the lane load was distributed cross the entire deck surface. The applied load is equal to the lane load calculated from the Strength I limit state. The two patches at the center of the deck mimic the two wheel loads. Since the purpose here is to investigate the maximum wheel load that the deck can sustain and to check the appropriateness of the deck thickness, the pressure applied on the wheel patches ranged from the AASHTO LRFD Strength I wheel load up to a value that was nearly six times larger. This allows for both assessment of performance under the standard loading as well as the determination of the maximum wheel pressure allowed for a certain deck thickness. Since the transverse bending and deck failure is localized, the effects of parameters such as the girder depth, bulb size and strand in bulbs are minimal and therefore are set to be constant for different deck thicknesses. The prestress in all the strands are set at 183.8 ksi (1366 MPa) and is kept constant for all models in this part of the study. These parameters are based on the cross-section for an 80-foot (24.38-m) span according to previous research.(2)

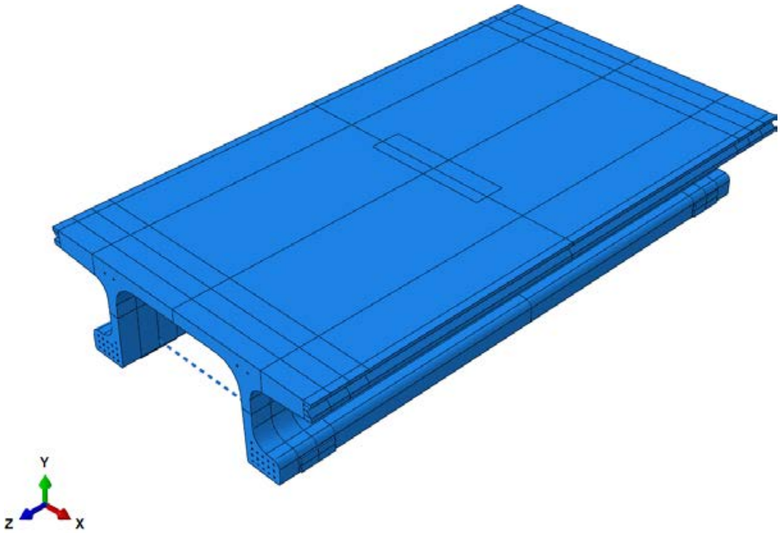

Figure 27. Illustration. Finite Element Model for Deck Thickness Analysis

Abaqus Results

There are two purposes in analyzing the effect of deck thickness. The first goal is to check whether certain deck thickness can meet the requirement of AASHTO LRFD loading under strength conditions. The second goal is to find the maximum possible wheel load that the deck can sustain for a particular deck thickness. In order to check whether the deck can perform satisfactory, the strain level under the AASHTO LRFD Strength I load condition was analyzed. The maximum principal strain under the load was used to check whether the girder can sustain the applied load. Figure 28 and Figure 29 (plotted using the same scale) shows the distribution of the principal tensile strain under the Strength I load for a typical model with regular diaphragms and very soft diaphragms, respectively. The figures present results from models having a deck thickness of 3.5 inches (89 mm). It can be seen that the critical section occurs at the middle of the deck, where the effect of transverse bending is most significant. The strain in the model with regular stiffness diaphragms is much smaller than the one with very soft diaphragms. A closer study on the strain in the transverse direction indicates that there exists inflection points in the deck for models with regular diaphragms and that the inflection is not apparent in the model with very soft diaphragms. The existence of inflection points indicates negative moment (in transverse bending) above the web which helps reduce the positive transverse bending at the critical section (the mid-deck). Figure 30 shows the strain in the transverse direction for the cross section at the midspan at different load levels. Given the neutral axis location and the near-linearity of the responses, it is clear that the transverse behavior of the deck is primarily in bending.

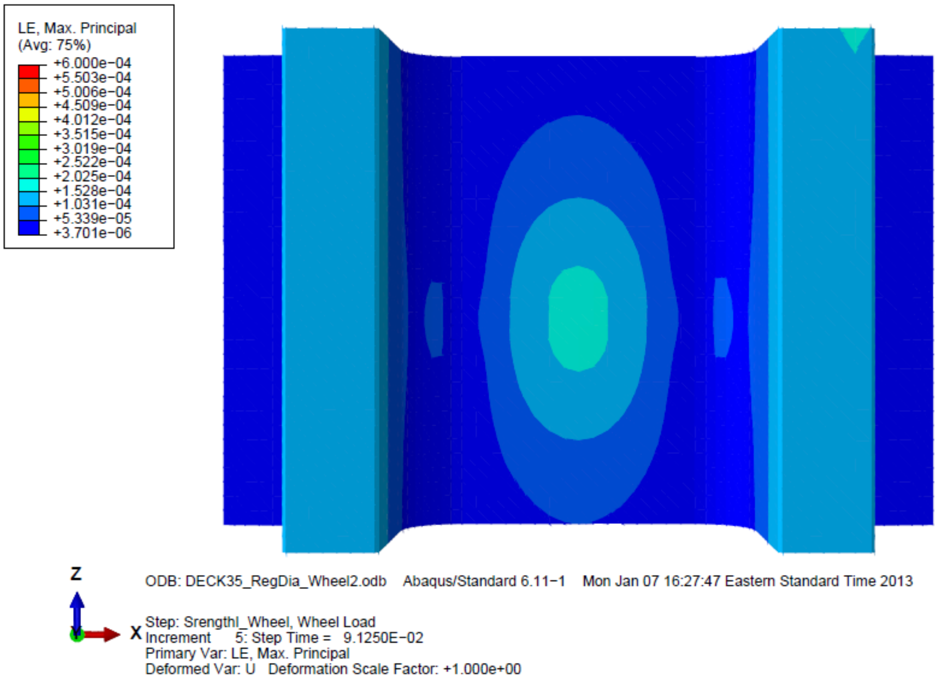

Figure 28. Illustration. Maximum Principal Tensile Strain for Regular Diaphragms Models

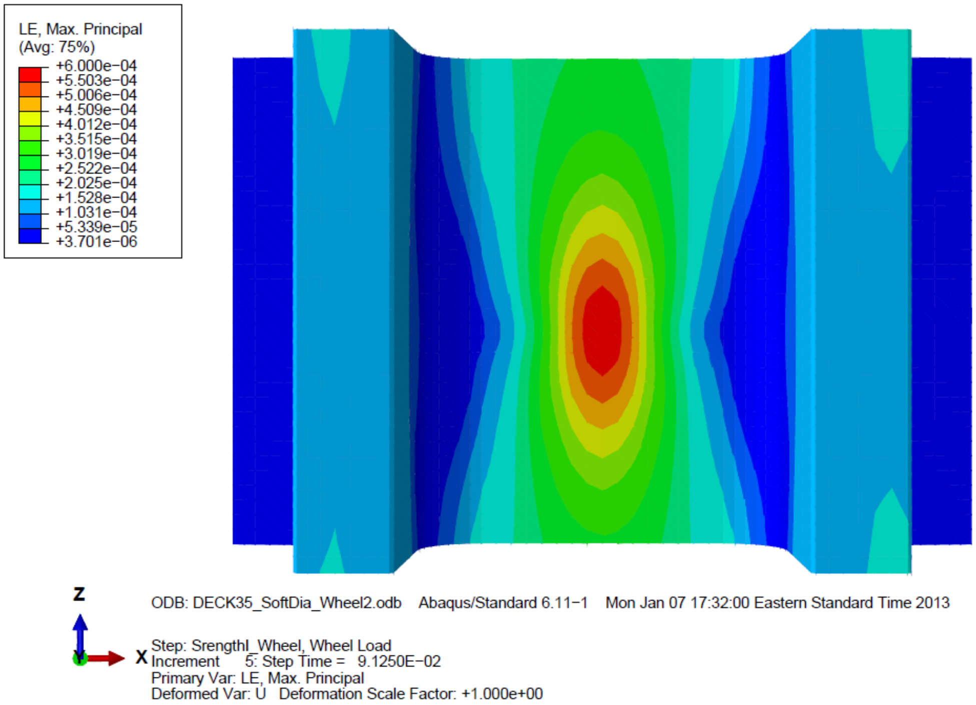

Figure 29. Illustration. Maximum Principal Tensile Strain for Soft Diaphragms Models

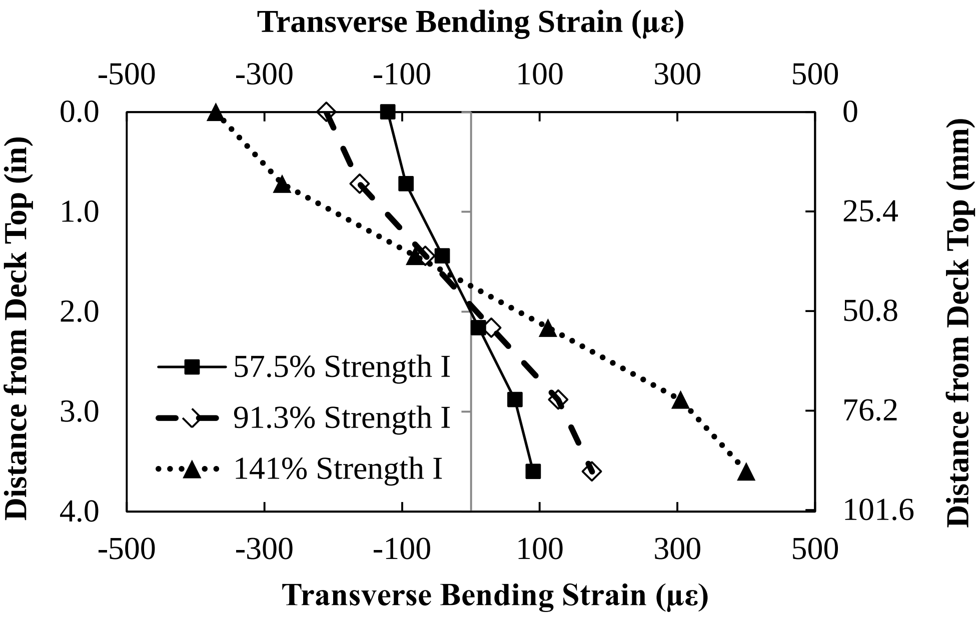

Figure 30. Illustration. Transverse Bending Strain along the Deck Height at Midspan

Table 6 summarizes the maximum tensile strain at midspan under the AASHTO LRFD Strength I load condition. The value in the table is obtained through linear interpolation using results from two closest time steps since the load applied in these steps is not exactly the standard Strength I load according to AASHTO LRFD. For example, if the strain was 176 με when the load is 91.25% of the Strength I load and became 41 με when the load is 141.2% of the Strength I load, the strain under Strength I load was determined to be 207 με using linear interpolation. It can be seen from the table that all three candidate thickness for the deck can sustain the loading without exceeding the strain limit. It can also be concluded that the stiffness of the diaphragms have a significant effect on the transverse bending behavior. The principal strain reduces greatly when a regular diaphragm was added. The diaphragm stiffness has a greater impact on the principal tensile strain for thinner decks. Based on these results and practical construction considerations, the 4.0 inch (102 mm) thick deck was selected for use throughout the remainder of the study.

Table 6. Maximum principal strain (με) at the midspan under Strength I load case.

Deck Thickness (inch (mm))	Maximum Principal Strain (με)		
	Stiff Diaphragm	Regular Diaphragm	Soft Diaphragm
4.5 (114)	149	152	252
4.0 (102)	182	191	363
3.5 (89)	196	207	756

In the investigation of maximum wheel pressure, two steps were used. In the first load step, the standard lane load was applied. In the second step, the wheel load was gradually increased from zero to 10 times the standard AASHTO wheel load. The limit state was defined as being the load when the maximum principal strain under the deck at midspan reaches the failure criteria, i.e. a tensile strain of 3000 με. Figure 31 shows the strain distribution of principal tensile strain near failure (when the strain is close to 3000 με) for the model with 4-inch thick deck and regular stiffness diaphragms. The strain distribution was similar to the distribution under Strength I load except that the magnitude of the strain value is greater.

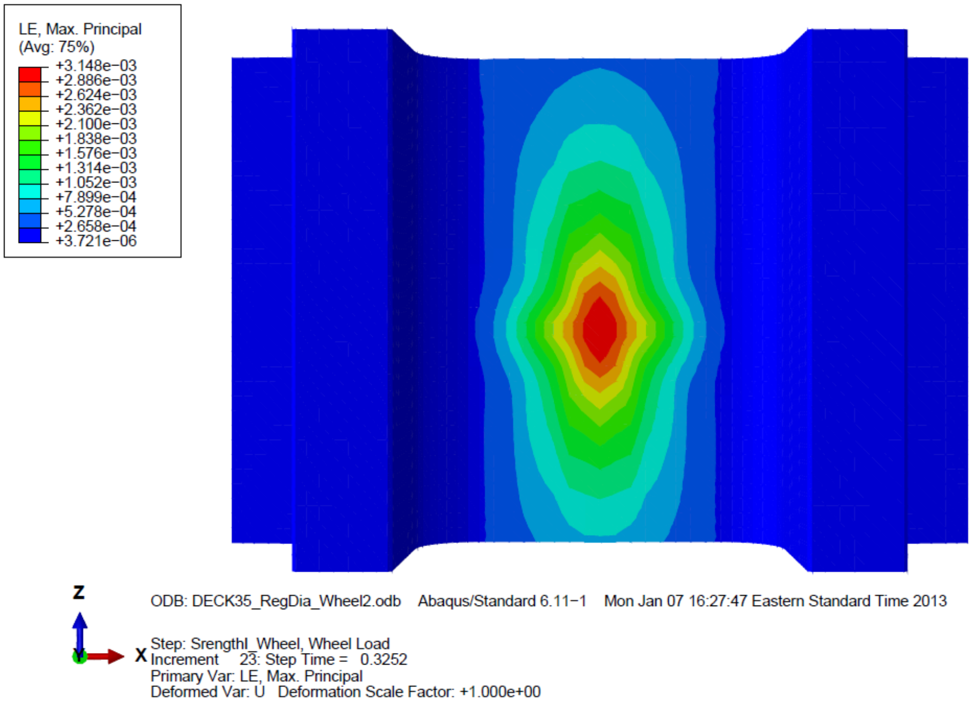

Figure 31. Illustration. Principal Tensile Strain at Midspan near Failure

Table 7 lists the results of maximum wheel load for different deck thicknesses. The load ratio in the table is defined as the ratio between the maximum wheel load and the AASHTO LRFD wheel load. It also should be noted that the value in the table is obtained through linear interpolation using results from two closest time steps. For example, if the strain was 2900 με when the load ratio is 2.8 and became 3500 με when the load ratio reached 3.2, the load ratio was determined to be 3.13 when the strain reaches 3000 με, according to linear interpolation. The results show that the introduction of the diaphragm increases the maximum wheel load significantly. The beneficial effect of the diaphragms was more significant in the models with a thinner deck (3.5 inches (89 mm)) than for models with a thicker deck (4.5 inches (114 mm)). All candidate thicknesses for the deck can sustain the requirement of AASHTO LRFD wheel load with a load ratio greater than 1.0. For simplicity and construction considerations, a 4-inch (102 mm) thick deck and along with regular stiffness diaphragms were used throughout the remainder of the report. For a 4-inch (102 mm) deck with a regular stiffness diaphragm at 15 feet

(4.57 m) spacing, the load ratio is 3.840. This indicates that the deck can sustain a wheel load 3.84 times the standard AASHTO wheel load, equivalent to a wheel load 61.44 kips (251 kN) of over a patch area of 20 inch by 10 inch (51 cm by 25 cm).

Table 7. Wheel load ratio when the limiting tensile strain is reached.

Deck Thickness (inch (mm))	**Load Ratio** **Stiff Diaphragm**	**Regular Diaphragm**	**Soft Diaphragm**
4.5 (114)	5.228	4.456	2.251
4.0 (102)	4.300	3.840	1.748
3.5 (89)	3.428	3.204	1.222

GLOBAL FLEXURAL AND SHEAR CAPACITYANALYSIS

The purpose of finding the deck thickness is to prevent local failure due to concentrated loads applied to the deck of the bridge. The next step is to develop appropriate cross-sections for a range of span lengths. In this section, the relationship between cross-section parameters and global flexural and shear behavior are investigated. The investigation allows a bridge designer to expand the current 2nd generation pi-girder sections to other span lengths. The new cross sections consider the cost-effective use of concrete bridge girder forming technology, thus engaging the common use of multiple formwork parts and requiring that certain cross-section parameters remain constant throughout the family of girders.

Cross-sectional Parameters

Figure 32 shows the profile of a 2nd generation pi-girder. To facilitate the efficient use of formwork, it is necessary to keep the slope of certain surfaces and fillet radii unchanged for all cross-sections in the development of the new cross sections. The surfaces whose slopes are kept constant are noted in Figure 32. The increment for girder height was determined to be 4 inches and the increment in the bulb size (height and width) was 2 inches in this research. In this way, a standard set of formwork with included filler pieces can allow for the fabrication of any of the girders cross sections. In addition, the thickness of the deck and the shape of the connection between girders remains the same for all cross-sections.

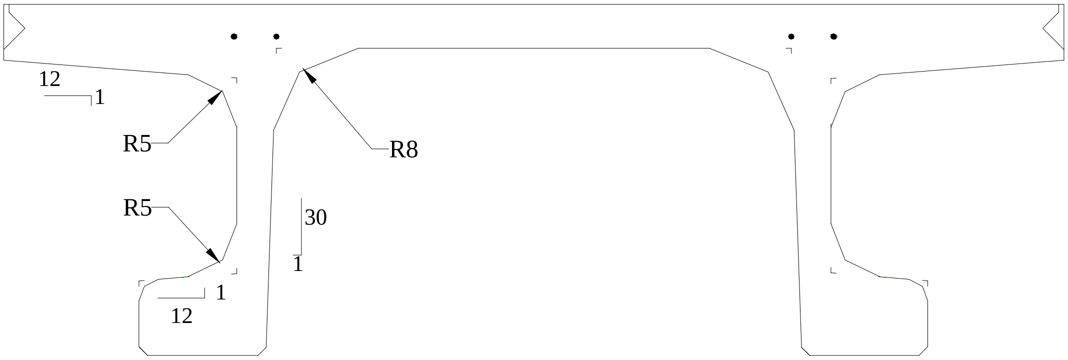

Figure 32. Illustration. Unchanged Parameters for Cross Section Series.

Factors Considered in the Finite Element Models

To investigate the global flexural behavior of a pi-girder, a single girder model was built using Abaqus. In addition to the cross sectional parameters, there are many factors can influence the flexural response of the pi-girder. Major factors considered in the finite element modeling include the effect of diaphragms and the load applied on the girder.

As mentioned in the previous section, the diaphragm has a significant effect on the transverse bending behavior of the section. The effect of the internal diaphragms on global flexure required further investigation. To investigate the effect of the diaphragm on a single girder model, the results of two finite element models were compared. In one model, two diaphragms were placed only at the two girder ends, simulating the case where no intermediate diaphragms are used. In the other model, eight intermediate diaphragms were placed at even spacing along the girder length, simulating the case where the diaphragms are more densely spaced. As a trial run, the span of the girder was arbitrarily determined to be 80 feet (20 m).

The maximum principal tensile strain at the mid-span was compared, as shown in Figure 33 and Figure 34. It can be seen that the effect of diaphragm on the flexural behavior of a single girder model is limited. The load versus mid-span deflection response for both cases is plotted in Figure 35. Again, the difference between the two cases is minimal. The reason for this is that for the longer span model, the longitudinal stiffness reduces and becomes relatively weaker compared with transverse bending. The longitudinal stiffness becomes the controlling factor. The diaphragms however primarily affect the stiffness in the transverse direction and have little influence on the global flexural behavior. Therefore, the effect of the diaphragms on the global flexure behavior is not apparent. According to this analysis, it was therefore reasonably conservative to model the single girder system using two diaphragms at ends without considering the intermediate diaphragm along the span.

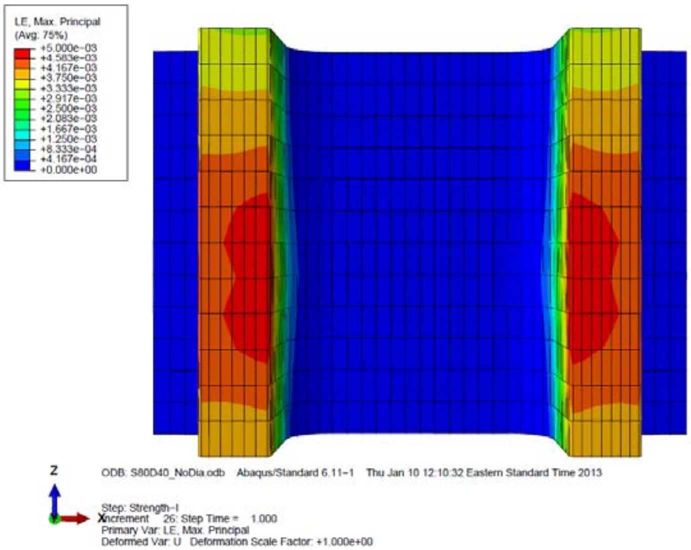

Figure 33. Illustration. Maximum Principal Strain at Midspan for Case 1.

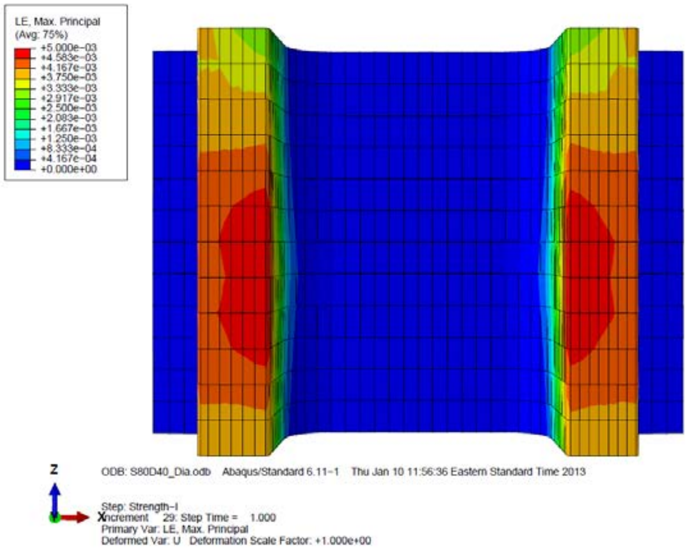

Figure 34. Illustration. Maximum Principal Strain at Midspan for Case 2.

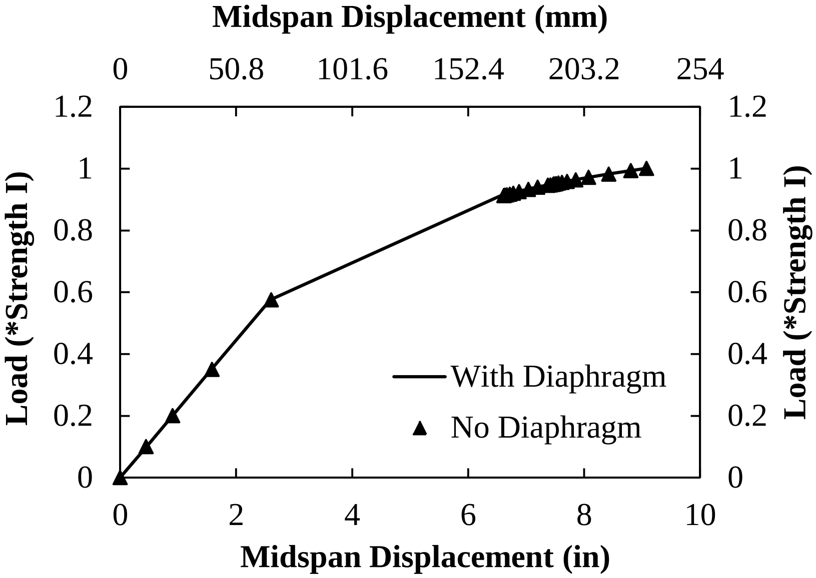

Figure 35. Illustration. Comparison of load versus midspan deflection response.

Another factor that needs to mention in the analysis of global flexural response of the single pi-girder model is the load pattern. In this research, the design truck was simulated by applying the entire load of the design truck at midspan. This simplification is conservative for the following reasons. First, the truck load applied on the model is on a standard design lane but the width of the girder is less than a design lane. Combining the three axles of wheel load into one axle load and placing the combined load at the midspan will create a larger flexural effect at the critical section, the midspan. It also should be noted that the model is a single girder model. This means that there is no adjacent girder resisting the load, i.e. no load distribution effect was considered. Even though it is possible that there are multiple trucks in the same lane, the chance for this scenario is very rare.

The location of the applied loads also affects the results. In the analysis of the global flexural behavior, the load was applied at the mid-span to create the maximum flexural effect. In the analysis of global shear behavior, the load was applied at a distance of three times the girder depth away from the support point in order to create a maximum shear response in the girder webs. Since this section focuses on the global behavior, the local failure mode should be suppressed. Unlike the previous section, the wheel load was applied above the web to suppress transverse bending failure. The magnitude of the load corresponds to the standard AASHTO Strength I wheel load.

Finite Element Model for Global Flexural and Shear Analysis

Figure 36 shows a typical three dimension model for the analysis of global flexural behavior. The girder was supported by 4 stiff springs at the end of each web in vertical direction and was supported by 4 soft springs in the transverse direction. In the longitudinal direction, the girder was fixed on one end and free on the other end. This simulates the simply supported boundary conditions. All elements and material properties are the same as the deck thickness analysis. The model for global shear behavior is the same as the model for flexural behavior except that the location of the load. The distance between support and the shear load was three times the depth of the girder.

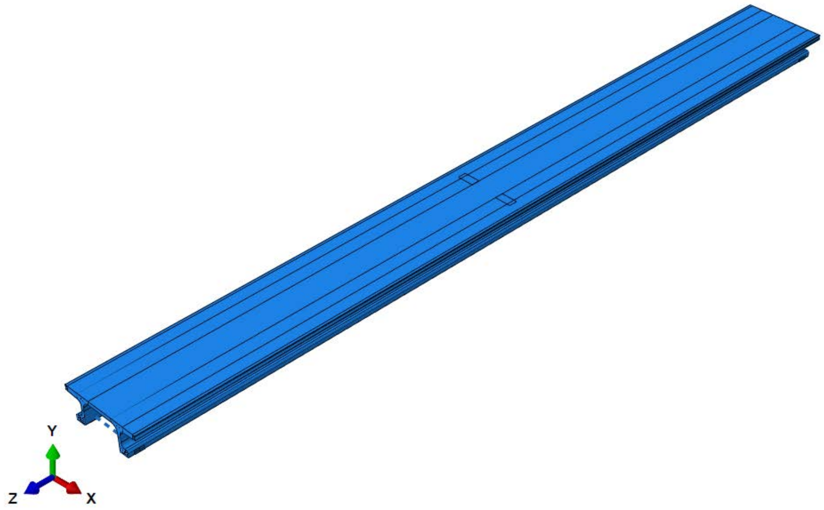

Figure 36. Illustration. Typical Finite Element Model for Global Flexure Analysis

Abaqus Results

It is known that the critical location for flexure is the midspan. Since the load is symmetric about the central axis of the cross section, only the distribution for half of the model is shown. Figure 37 shows the stress distribution of principal tensile strain for models under load for global flexure at the midspan. It should be noted that the stress and strain results in this section result from the combined effect from prestress, dead loads and live loads. It can be seen that the maximum strain occurs at the bottom of the bulb, indicating that bulb bottom is the critical location for global flexure. The longitudinal stress in a typical prestress strand is shown in Figure 38. It is clear that the critical location for both concrete and prestress strand under flexure load is at the midspan. The critical location for the shear is between load and the closest support (called shear span). The maximum principal tensile strain distribution for the shear span under shear loads was shown in Figure 39. From the figure, it is clear that the maximum shear strain occurs in the web and in the transition area from the web to the bulb.

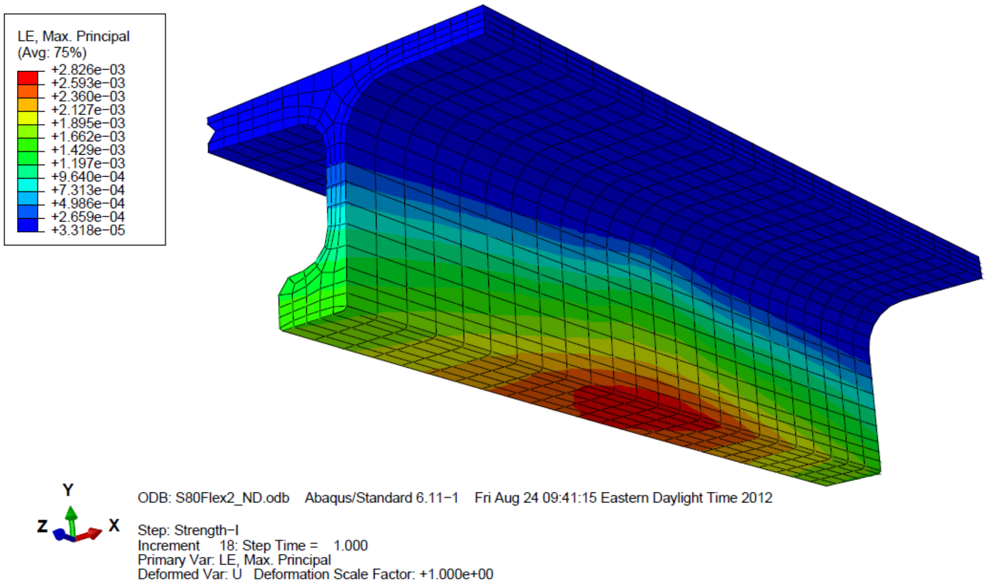

Figure 37. Illustration. Principal Tensile Strain for Global Flexure Analysis

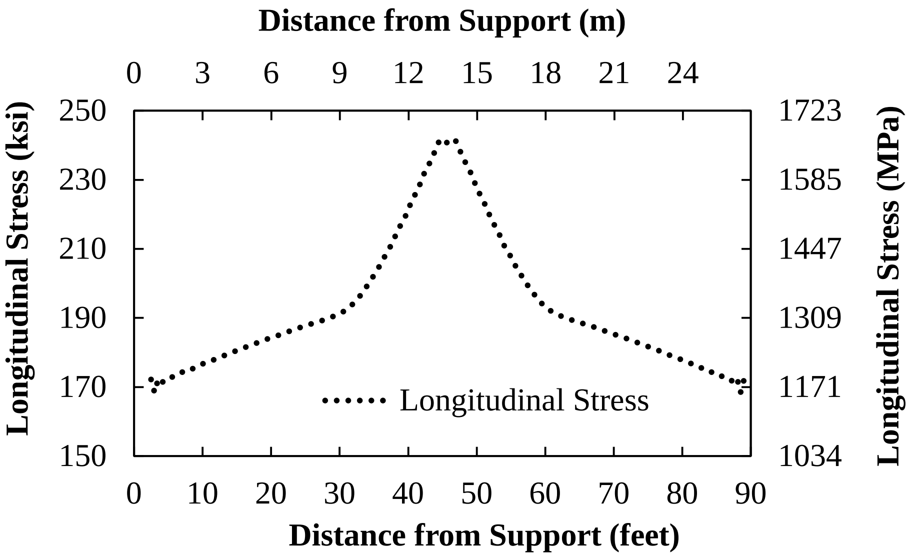

Figure 38. Illustration. Longitudinal Stress in Strands for Global Flexure Analysis

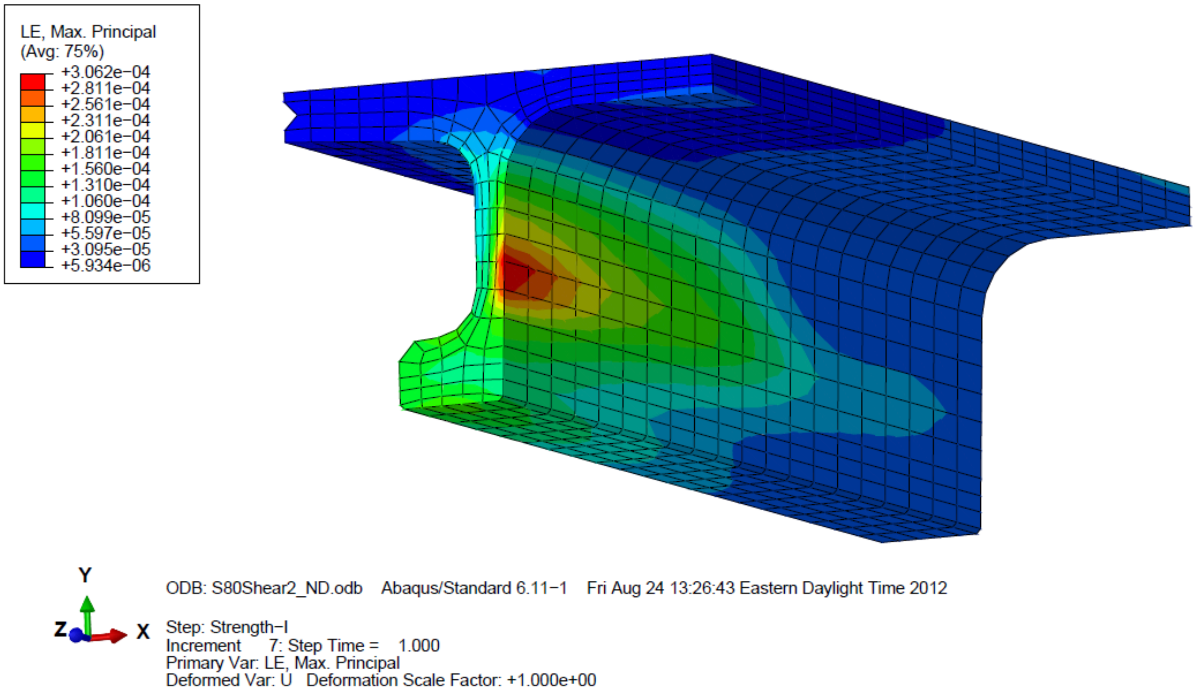

Figure 39. Illustration. Principal Tensile Strain for Global Shear Analysis

Through an iterative process, cross section that can meet the requirement of AASHTO Strength I limit state were developed and are shown in Table 8. In the table, the strand layout is referenced by the number of strands in each row starting from the bottom. For example, layout "6-6-6-6-2" means there are five layers of strands in the bulb. The first four layers from the bottom have 6 strands and the fifth layer from the bottom has 2 strands. It should be noted that the size for Section II through IV is controlled by the deflection (discussed in the next section), therefore the strain level is relatively low compared with other cases. The details about the cross sections are shown in Figure 40 to Figure 43. The maximum principal strains under Strength I load for all cross section at the target span length are less than 3000 με and meet the requirements defined earlier in this report.

Table 8. Summary of cross section responses with all strand locations filled for different span lengths.

Section ID	Section I	Section II	Section III	Section IV
Span (feet (m))	80 (24.4)	95 (29.0)	105 (32.0)	135 (41.1)
Girder Depth (in. (mm))	35 (889)	39 (991)	43 (1092)	47 (1194)
Strands per Girder	36	46	56	68
Deck Width (in. (mm))	100 (2540)	100 (2540)	104 (2642)	104 (2642)
Web Thickness (in. (mm))	3.37 (85.6)	3.33 (84.5)	5.27 (133.8)	5.23 (132.8)
Bulb Width (in. (mm))	12.03 (305.6)	11.90 (302.3)	13.77 (349.8)	13.63 (346.2)
Bulb Height (in. (mm))	7.25 (184.2)	9.25 (235.0)	9.16 (232.7)	11.25 (285.8)
Strand Layout	5-5-5-1	5-5-5-5-1	6-6-6-6-2	6-6-6-6-6-2
Flexure: Maximum Tensile Strain at Midspan (με)	2826	1792	902	1719
Flexure: Maximum Longitudinal Stress in Strands (ksi (Mpa))	251 (1730)	230 (1586)	208 (1434)	229 (1579)
Shear: Maximum Tensile Strain in the Web (με)	457	291	159	189

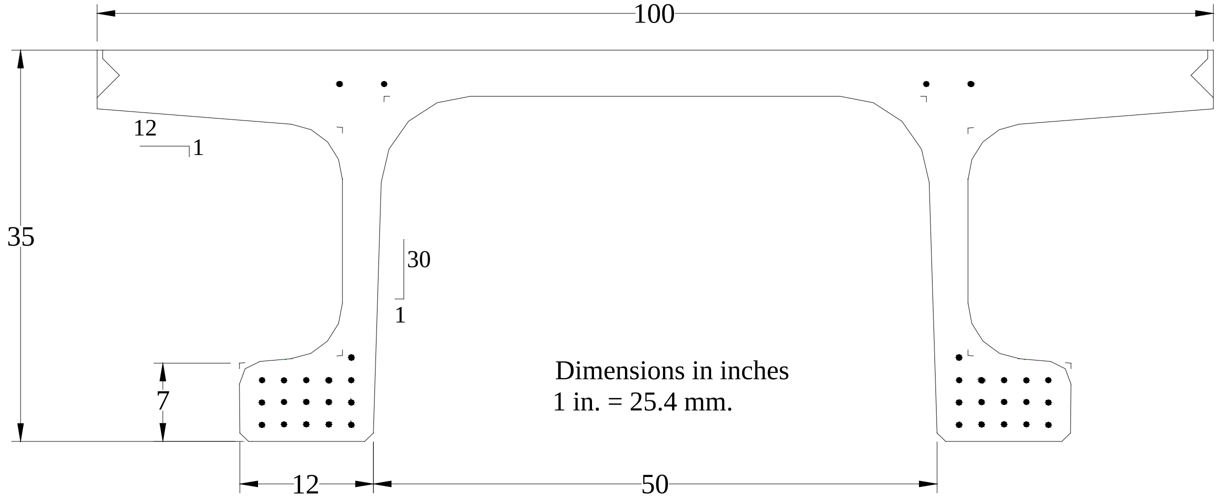

Dimensions in inches
1 in. = 25.4 mm.

Figure 40. Illustration. Section I for Spans up to 80 feet (24.4 m)

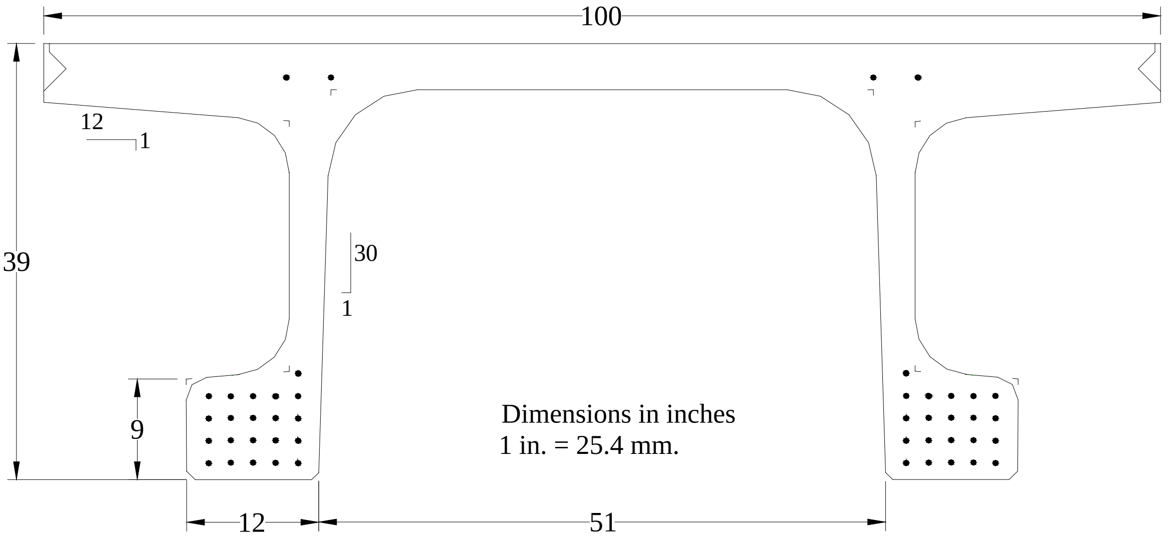

Figure 41. Illustration. Section II for Spans up to 95 feet (29.0 m)

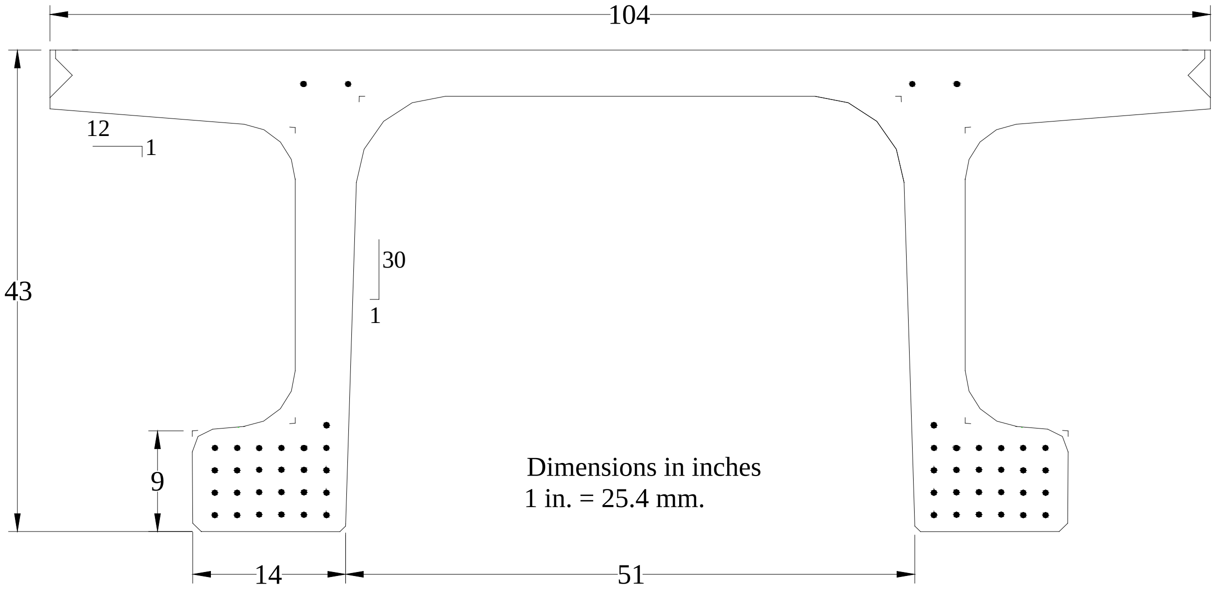

Figure 42. Illustration. Section III for Spans up to 105 feet (32.0 m)

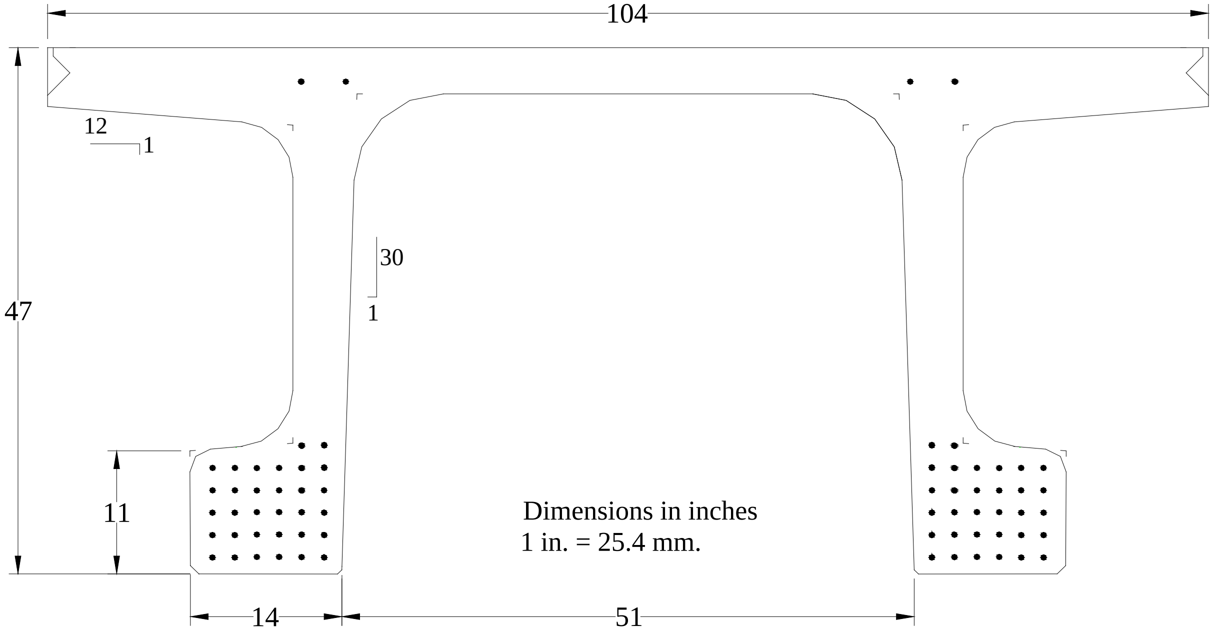

Figure 43. Illustration. Section IV for Spans up to 135 feet (41.1 m)

Refinement of Cross Sections

As indicated in Table 8, the strain values for Sections II through IV under Strength I load are relatively small. This indicates that some of the strands could be eliminated. It is therefore necessary to check whether it is possible to reduce the number of strands in the deflection controlled cross-sections. It is further necessary to investigate the relationship between the maximum span and the number of strand for each cross-section type. The shear capacity was not considered in this portion of the analysis. There are two reasons for this. First, the shear capacity was controlled by the size of the section and prestressing strands did not impart a significant influence on the shear capacity. Second, global shear analysis showed that the strain level for every cross section in global shear analysis is very small compared with flexural analysis indicating that the cross section is controlled by flexure. When removing “extra” strands from the section, preference were given to strands further from the bottom which are less efficient in terms of flexural capacity. The single girder model was reused to check the load capacity of the refined sections. The strand layouts in the bulb for the refined cross section for each span are shown in Figure 44 through Figure 47. Table 9 summarizes the results for the refined cross sections. It is noted that the refined Section I was unchanged because this section was controlled by the flexural strength.

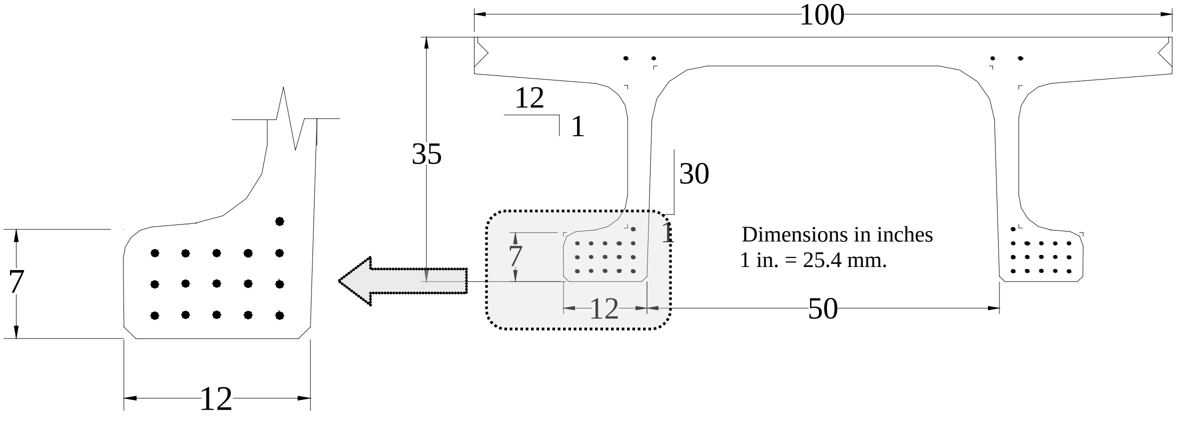

Figure 44. Illustration. Strand Layout of Section I for 80-foot (24.4-m) Span

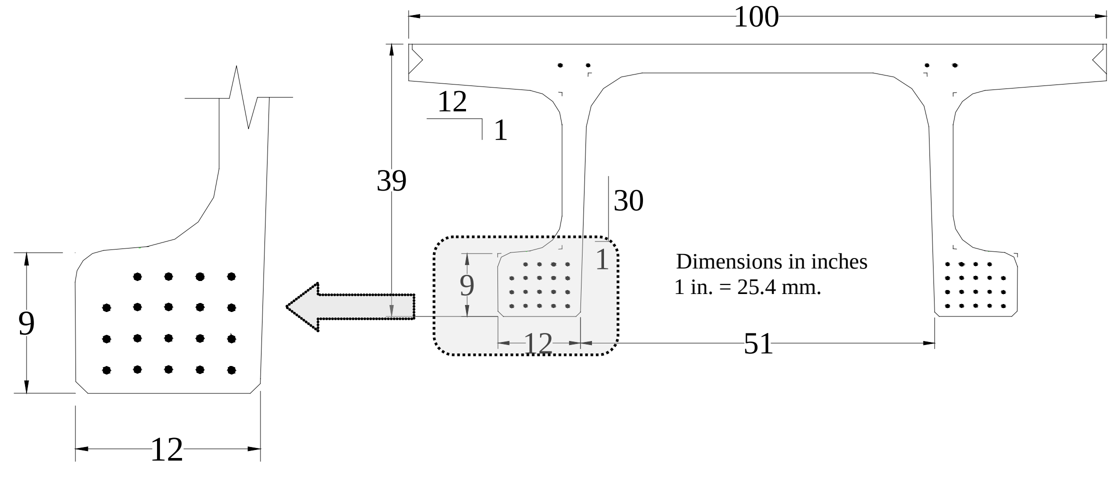

Figure 45. Illustration. Strand Layout of Section II for 95-foot (29.0-m) Span

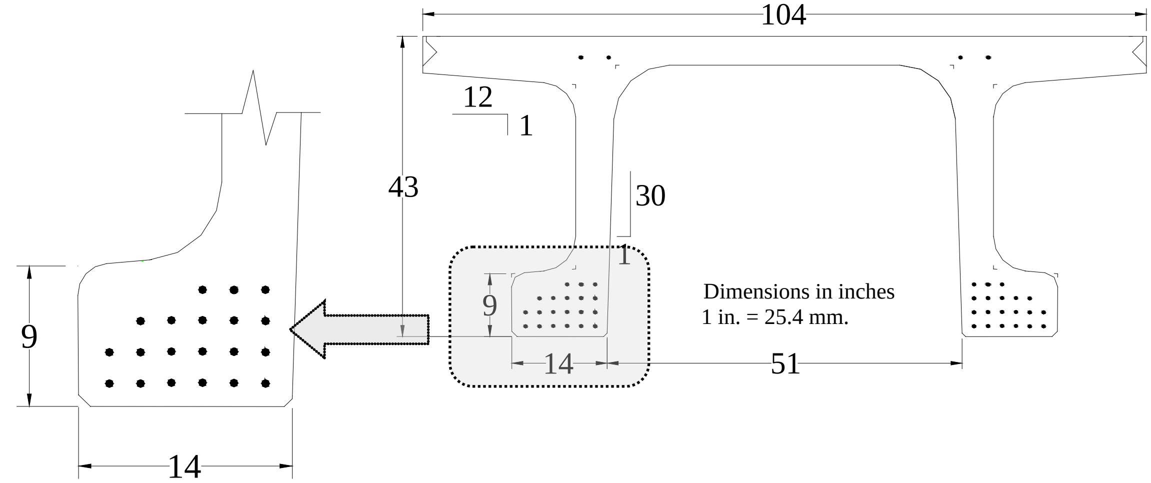

Figure 46. Illustration. Strand Layout of Section III for 105-foot (32.0-m) Span

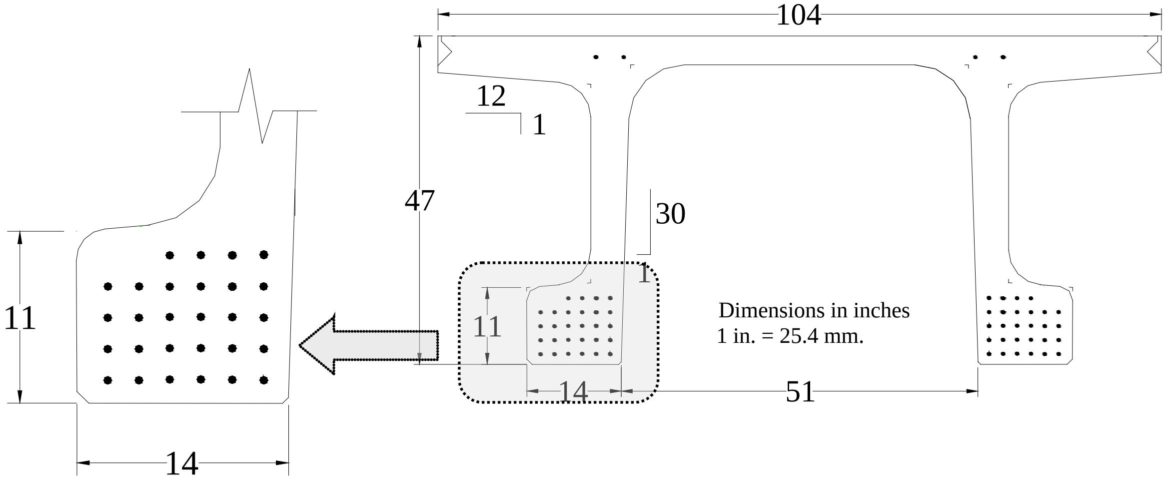

Figure 47. Illustration. Strand Layout of Section IV for 135-foot (41.1-m) Span

Table 9. Refined cross sections for different span lengths.

Section ID	Section I	Section II	Section III	Section IV
Span (feet (m))	80 (24.4)	95 (29.0)	105 (32.0)	135 (41.1)
Girder Depth (in. (mm))	35 (889)	39 (991)	43 (1092)	47 (1194)
Strands per Girder	36	42	44	60
Deck Width (in. (mm))	100 (2540)	100 (2540)	104 (2642)	104 (2642)
Web Thickness (in. (mm))	3.37 (85.6)	3.33 (84.5)	5.27 (133.8)	5.23 (132.8)
Bulb Width (in. (mm))	12.03 (305.6)	11.90 (302.3)	13.77 (349.8)	13.63 (346.2)
Bulb Height (in. (mm))	7.25 (184.2)	9.25 (235.0)	9.16 (232.7)	11.25 (285.8)
Strand Layout	5-5-5-1	5-5-5-4	6-6-5-3	6-6-6-6-4
Flexure: Maximum Tensile Strain at Midspan (με)	2826	2531	2520	2694
Max Longitudinal Stress in Strands (ksi (MPa))	251 (1730)	247 (1703)	248 (1710)	250 (1724)

DEFLECTION CHECK UNDER LIVE LOADS

In addition to the strength limit state, AASHTO LRFD also contains language speaking to the flexibility of the structure under live load. The deflection should be taken as the larger of the deflection due to design truck alone or due to 25% of the design truck together with the design lane load. The impact factor should be considered when calculating the loads. The requirement on the deflection should be limited to 1/800 of the span length. This portion of the report checks whether the deflection of the proposed sections can meet the requirement specified in AASHTO.

Factors Considered in the Finite Element Models

As mentioned in previous section, the single girder model was conservative in terms of deflection. It is therefore necessary to develop a more realistic model to evaluate the live load deflection. In this section, a 3-girder bridge model was used. The deck widths of the developed cross sections are 100 inches (2.54 m) or 104 inches (2.64 m). A three-girder system is enough to accommodate two traffic lanes. It is conservative compared with other combinations of girder numbers and lane numbers. For example, three traffic lanes require a minimum of five girders. Two additional girders are needed to accommodate one additional lane. With the introduction of adjacent girders, the load will be distributed to and resisted by other girders. Therefore, the maximum deflection is reduced. For simplicity, the interface between adjacent girders in the 3-girder model was assumed to be perfectly bonded, i.e., no slip occurs at the interface. Although not necessarily conservative, this assumption is reasonable since experimental results have demonstrated that the development length for rebar in UHPC is very short and it is possible to develop a joint that emulated cast-in-place bridge deck construction.(24) The magnitude for traffic load was defined in AASHTO LRFD, but the location or pattern of the applied load also have influence on the deflection. Figure 48 shows the relative location of the wheel load and lane load. This load pattern creates maximum possible deflection at the exterior web/leg in the exterior girder.

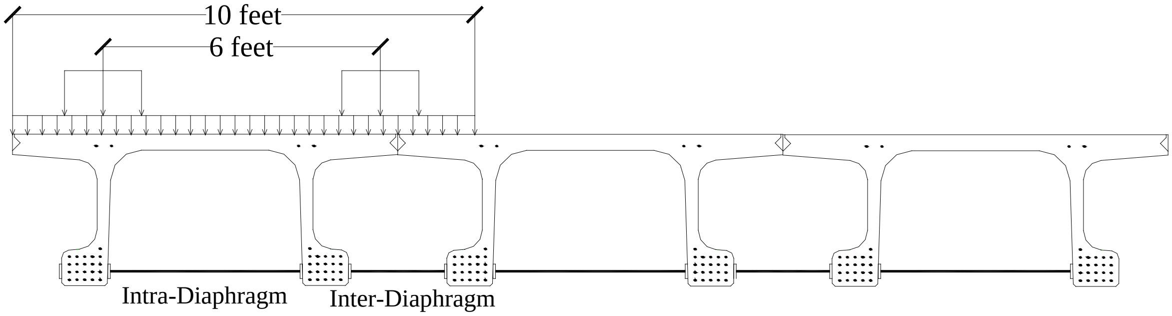

Figure 48. Illustration. Load Pattern for Deflection Check under Live Load

In the analysis of flexural and shear capacity of a single girder, the diaphragms do not have significant effect because they provide minimal contribution to the longitudinal strength. However, in the analysis of the deflection, diaphragms will have an effect because they influence the distribution of the loads among different girders. In this research, a diaphragm spacing of 15 feet (4.57m) was used. This diaphragm spacing was selected based on previous experience in the field.(17) There are two types of diaphragms in the model for deflection check. The intra-diaphragm is the diaphragm that connects the two "legs" within the same pi-girder piece and the inter-diaphragm refers to the diaphragm that connects the adjacent girders. The inter- and intra-diaphragms were placed at the same location along the longitudinal direction of the girder. The stiffness of the inter-diaphragm was the same as those used in previous analysis. The stiffness of the intra-diaphragm was calculated based on the length of the diaphragm using the equation for springs in series. The diaphragms were modeled in Abaqus by using connector elements. A typical finite element model for live load deflection is shown in Figure 49. The crosses in the figure show the locations of the diaphragms.

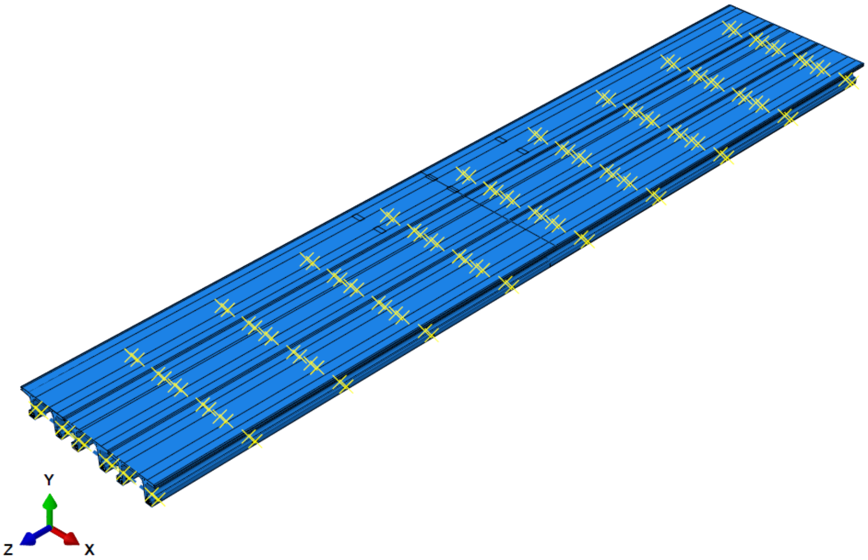

Figure 49. Illustration. Finite Element Model for Live Load Deflection Check

Abaqus Results

Figure 50 shows the typical deflection shape at the mid-span under service load. The deformed shape (with prestress, dead and live load) is shown as the shaded area and the undeformed shape (no prestress, no dead and live load) is shown as the dashed lines. It can be seen that the sections deflected and rotated due to the eccentricity of the live load (the load was applied on the exterior girder on the right). This indicates that the adjacent girder helps distribute across the entire bridge system. The property of the connection plays an important role in distributing the load transversely. The influence of the connection properties on the load distribution is beyond the scope of this research.

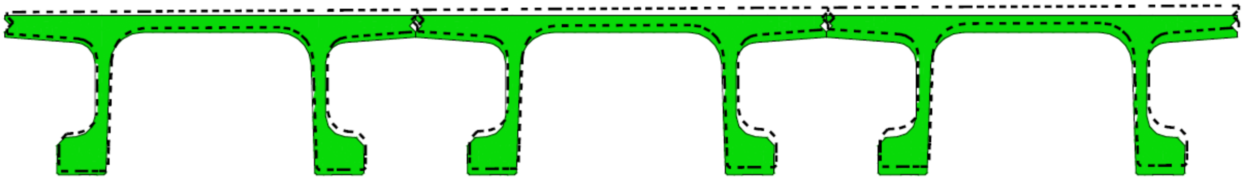

Figure 50. Illustration. Typical Deformation at the Midspan under Service Loads

The deflections under live load (truck load only and lane load plus 25% truck load) for different models are summarized in Table 10. From the table, it can be seen that deflection ratios for all models are less than L/800 (i.e., deflection/span < 1/800 = 0.00125 = 0.125%) and therefore, the deflection requirements were satisfied. It also can be observed that the deflection from the truck load controls the results of deflection analysis.

Table 10. Summary of live load deflection for sections for full strands.

Span (feet (m))	Truck Load Only		Lane Load plus 25% Truck Load	
	Deflection (inch (mm))	Deflection/Span Ratio (%)	Deflection (inch (mm))	Deflection/Span Ratio (%)
80 (24.4)	1.13 (28.7)	0.118	0.64 (16.3)	0.078
95 (29.0)	1.34 (34.0)	0.118	0.96 (24.4)	0.084
105 (32.0)	1.50 (38.1)	0.119	1.00 (25.4)	0.079
135 (41.1)	1.98 (50.3)	0.122	1.74 (44.2)	0.107

By combining the results on global flexural and shear capacity (Table 8) and live load deflection (Table 10), it can be seen that the controlling factors for the optimized cross-section varies from case to case. For the case of the 80-foot (24.4m) span, it is the strength limit that determines the cross-section sizes; however, the controlling factor for the cross-section in the cases of 95 feet (29.0 m), 105 feet (32.0 m) and 135 feet (41.1m) spans is the deflection. This indicates that for longer span, the UHPC pi-girder cross sections are determined by the stiffness and not by strength.

The live load deflection was also checked for the refined cross sections. The FE model used was the same as one used in the previous section except that the cross section was replaced with the refined cross sections. Table 10 indicates that the deflection was controlled by the truck load only for all cases. Therefore only the deflection under truck load was checked in this section. Table 11 summarizes the deflection check results for the refined cross-sections. Combining Table 9 and Table 11, it can be seen that strain under Strength I load for all cross sections are less than 3000 $\mu\varepsilon$ and the deflection under live load is less than the 0.125% of the span length. Therefore, all the refined cross sections passed the strength and deflection check.

Table 11. Deflection under truck loads for refined cross sections.

Section ID	Section I	Section II	Section III	Section IV
Span (feet (m))	80 (24.4)	95 (29.0)	105 (32.0)	135 (41.1)
Midspan Deflection (inch (mm))	1.13 (28.7)	1.35 (34.3)	1.51 (38.4)	1.98 (50.3)
Deflection/Span (%)	0.118	0.118	0.120	0.122

MODIFIED CROSS SECTIONS FOR SHORTER SPANS

In practice, the bridge span may not be the same as the target span evaluated in the previous sections. To facilitate use of these results, it is necessary to investigate the possible span range for each type of cross sections. The span lengths in the previous sections were the maximum possible span for each cross section. The applicability of cross sections on smaller spans needs to be studied. To achieve this, a parameter analysis was conducted to find the maximum span for sections with the same depth but different strand layouts. It is possible that strands be eliminated by using a deep cross section on a short span. However, this may not be cost effective or geometrically appropriate for the particular site under consideration. In this research, only a limited span range was investigated for each section. Since each section was applied on a shorter span, the deflection requirement was automatically satisfied since the flexural stiffness increases as the span decreases. The single bridge model similar to those for global flexural analysis under Strength I load was used in this portion of the study. The shear capacity was not checked in this section as the shear load was unchanged. The results of using the section with fewer strands on a shorter span are summarized in Table 12. Combining results from previous sections, Figure 51 shows a graphic representation of the applicable span range for each girder depth. Table 13 summarizes the cross-sectional properties and applicable span range of the proposed cross sections.

Table 12. Modified cross sections for application on smaller span length.

Section ID	**Section I**	**Section II**	**Section III**	**Section IV**
Span (feet (m))	70 (21.3)	75 (22.9)	80 (24.4)	100 (30.5)
Girder Depth (in. (mm))	35 (889)	39 (991)	43 (1092)	47 (1194)
Deck Width (in. (mm))	100 (2540)	100 (2540)	104 (2642)	104 (2642)
Web Thickness (in. (mm))	3.37 (85.6)	3.33 (84.5)	5.27 (133.8)	5.23 (132.8)
Bulb Width (in. (mm))	12.03 (305.6)	11.90 (302.3)	13.77 (349.8)	13.63 (346.2)
Bulb Height (in. (mm))	7.25 (184.2)	9.25 (235.0)	9.16 (232.7)	11.25 (285.8)
Strand Layout	5-5-3	5-5-2	6-6-3	6-6-3
Flexure: Maximum Tensile Strain at Midspan (με)	2301	2326	2273	2285
Max Longitudinal Stress in Strands (ksi (MPa))	244.0 (1862)	244.1 (1863)	243.8 (1681)	243.7 (1680)

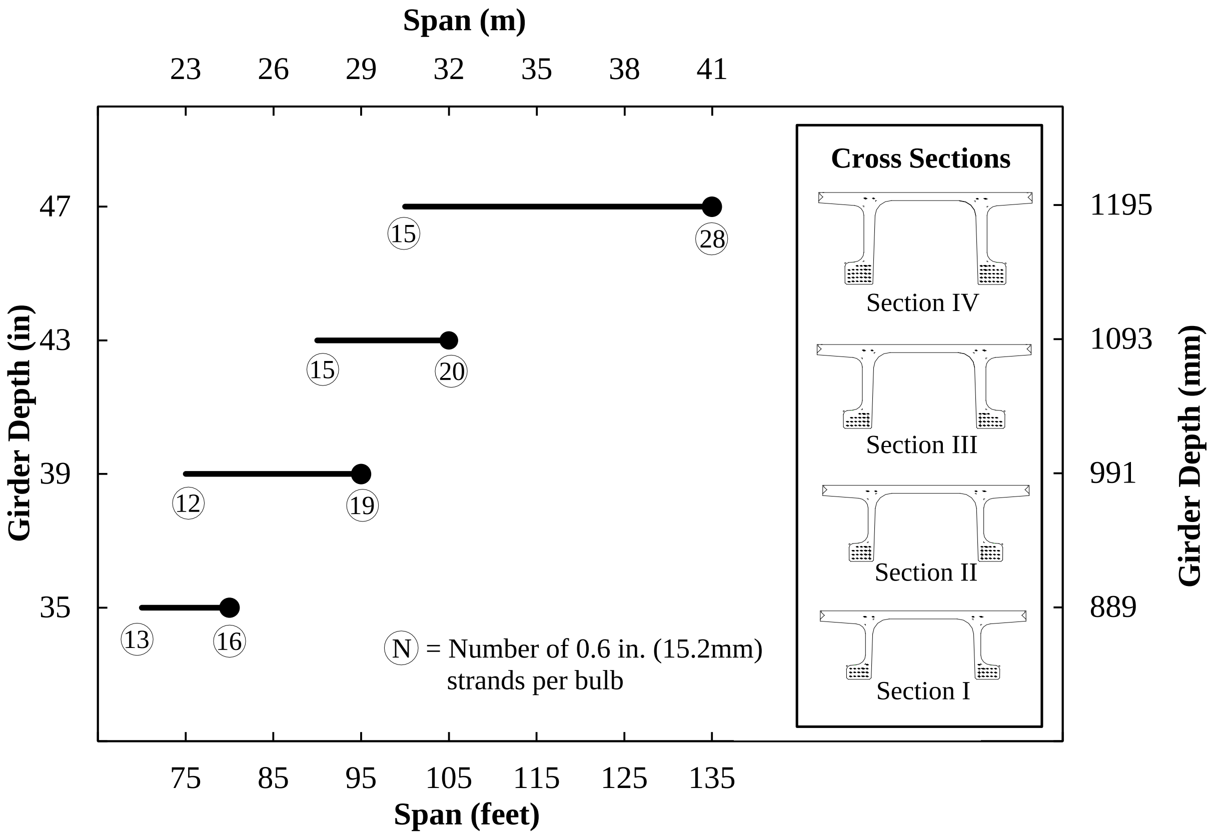

Figure 51. Illustration. Summary of Developed Cross Sections

Table 13. Properties of the proposed cross-sections.

Section ID	Section I	Section II	Section III	Section IV
Girder Depth (in.)	35	39	43	47
Girder Depth (mm)	889	991	1092	1194
Area (in^2)	877	935	1126	1200
Area ($\times 10^4$ mm^2)	56.6	60.3	72.7	77.4
Moment of Inertia ($\times 10^9$ in^4)	1.50	1.84	1.94	2.38
Moment of Inertia ($\times 10^{14}$ mm^4)	6.24	7.66	8.07	9.90
Weight (lb/ft)	944	1006	1212	1291
Weight (kN/m)	13.77	14.69	17.69	18.85
Span Range (feet)	70~80	75~95	80~105	100~135
Span Range (m)	21.3~24.4	22.9~29.0	24.4~32.0	30.5~41.4

SUMMARY OF THE CHAPTER

This chapter extrapolates the cross-sections of the 2nd generation UHPC pi-girder to accommodate larger span length by revising the deck thickness, girder height, bulb width and height, and web thickness, as well as the number of pre-stress strands in the bulb.

A single girder model with a short span was used to investigate the effect of deck thickness while suppressing other types of failure. It was found that the transverse bending failure was the controlling factor for the deck thickness. The maximum wheel load for 4-inch (102 mm) deck thickness is 1.75 times the AASHTO LRFD (Strength I) wheel load when there is no diaphragm and is significantly increased when diaphragms are included.

Four cross-sections were developed and the global flexure and shear behavior was investigated by finite element modeling of single girder systems. For simplicity, the global behavior was investigated using a single girder model with the actual span lengths. The single girder model does not consider the load distribution effect of adjacent girders and therefore is more conservative. The dimensions of the section were investigated through an iterative approach that combined global flexure and shear. The results showed that the proposed sections, all of which have superstructure depths of 47 inches (1.19 m) or less, can accommodate span length up to 135 feet (41.1m) under AASHTO LRFD Strength I load and simply supported conditions.

The proposed cross sections developed were further evaluated for deflection under live load according to AASHTO LRFD. To fully evaluate the deflection, a 3-girder bridge system was modeled using finite element analysis. This is a conservative but more realistic situation. The deflection was calculated as the difference in the deflection before and after the application of live load. The ratio between the deflection and the span length was calculated and compared with the criteria defined in AASHTO. The results showed that all cross-sections and models meet the deflection requirements under live load.

The applicability of the proposed cross sections on shorter spans was also investigated using finite element methods. Only the behavior under Strength I load was considered as the deflection requirement was satisfied automatically due to the shorter span length. A design chart was provided to facilitate appropriate cross section selection during preliminary design.

CHAPTER 5. CONCLUSIONS AND FUTURE WORK

INTRODUCTION

Compared with traditional concrete, UHPC exhibits enhanced mechanical and durability properties that afford opportunities to reconsider common structural component configurations. It is necessary to develop optimized cross-sections in order to efficiently utilize this high performance material. The object of this research was to develop a family of prestressed concrete girders accommodating a range of span lengths. Finite element analysis was used in this research to perform an analysis on different cross-sectional parameters.

This computational investigation focused on the development of the optimized cross-section for simply supported UHPC pi-girders with span length up to 135 feet (41.1 m). The finite element model was built and calibrated by comparing the experimental results with the simulated results. A parameter analysis was then conducted based on the calibrated finite element model. The analysis focused on the evaluation of transverse bending capacity, global flexural and shear capacity, as well as the deflection under live load. Four different cross-sections were developed.

CONCLUSIONS

The following conclusions are presented based on the research presented in this report.

1. The behavior of the UHPC can be appropriately modeled through the use of the existing concrete damage plasticity model within the finite element software package. The finite element model was capable of re-producing load-displacement and strain responses with reasonable accuracy and therefore is considered valid for further analysis.

2. The results from the parameter analysis on the deck thickness showed that the stiffness of the diaphragm impacts the transverse bending capacity of the pi-girders. Even though a deck thickness of 3.5 inches (89 mm) was sufficient to resist standard AASHTO load (Strength I), a deck thickness of 4 inches (102 mm) is recommended considering construction tolerances and the potential for non-standard vehicle configurations causing large localized loadings on the deck.

3. A diaphragm spacing of 15 feet (4.57m) for both inter-diaphragm and intra-diaphragm is recommended based on previous experience and analysis. Diaphragms play an important role in the transverse bending behavior, especially for a thinner deck. The effect of the diaphragm on the distribution of the load among adjacent girders is important. However, the effect of diaphragms becomes less significant for global flexural behavior, especially for long-span models. The reason is that the stiffness in the longitudinal direction reduces significantly as the span increases and the behavior is controlled by the longitudinal stiffness.

4. A family of UHPC pi-girders was developed for spans ranging up to 135 feet (41.1 m). These decked girders, with depths of 47 inches (1.19 m) or less, were designed to

resist loads in excess of those required by the AASHTO LRFD Bridge Design Specifications while meeting the live load deflection recommendations.

5. The proposed sections can be applied on shorter spans by reducing the number of prestress strands in the bulb. A design chart was provided based on the parameter analysis using finite element method. The chart can facilitate the selection of cross sections in the preliminary design stage.

FUTURE RESEARCH

The research discussed herein presents a foundation on which future advancements can be built. Potential future studies include the following:

1. The distribution factor for bridge system with pi-sections needs to be evaluated. The effect of diaphragm stiffness and diaphragm spacing on the distribution factor of pi-girder system needs further investigation.

2. The UHPC pi-girder concepts investigated herein may be appropriate for extension into both multi-span continuous structures and post-tensioned structures.

REFERENCES

1. Association Française de Génie Civil, Interim Recommendations for Ultra High Performance Fibre-Reinforced Concretes, 2002.
2. L. Chen, and B. Graybeal, “Finite Element Analysis of Ultra-High Performance Concrete: Modeling Structural Performance of an AASHTO Type II Girder and a 2nd Generation Pi-Girders,” Federal Highway Administration, NTIS Accession No. PB2011-100864, October 2010, 177 pp.
3. Chen, L., and Graybeal, B., "Modeling Structural Performance of Ultra-High Performance Concrete I-Girders," *ASCE Journal of Bridge Engineering*. V. 17, No. 5, September-October 2012, pp. 754-764.
4. Chen, L., and Graybeal, B., "Modeling Structural Performance of 2nd Generation Ultra-High Performance Concrete Pi-Girders," *ASCE Journal of Bridge Engineering*. V. 17, No. 4, July-August 2012, pp. 634-643.
5. Graybeal, B., “Structural Behavior of Ultra-High Performance Concrete Prestressed I-Girders,” Federal Highway Administration, Report No. FHWA-HRT-06-115, August 2006, 104 pp.
6. Graybeal, B., “Material Property Characterization of Ultra-High Performance Concrete,” Federal Highway Administration, Report No. FHWA-HRT-06-103, August 2006, 186 pp.
7. Graybeal, B., “Compressive Behavior of Ultra-High Performance Fiber-Reinforced Concrete,” *ACI Materials Journal*, V. 104, No. 2, March-April 2007, pp. 146-152.
8. Graybeal, B., and Baby, F., “Development of a Direct Tension Test Method for Ultra-High-Performance Fiber-Reinforced Concrete,” *ACI Materials Journal*, V. 110, No. 2. March-April 2013, pp. 177-186.
9. Chuang, E., “Ductility Enhancement of High Performance Cementitious Composites and Structures,” Massachusetts Institute of Technology, 2002, 319 pp.
10. Graybeal, B.A., “Structural Behavior of a Prototype Ultra-High Performance Concrete Pi-Girder,” Federal Highway Administration, NTIS Accession No. PB2009-115495, 2009, 145 pp.
11. Behloul, M., G. Causse, and D. Etienne, “Ductal® Footbridge in Seoul,” First fib Congress, Osaka, Japan, October 2002, 11 pp.
12. Chuang, E., and F. Ulm, “Two-Phase Composite Model for High Performance Cementitious Composites,” *Journal of Engineering Mechanics*, V. 128, No. 12, 2002, pp. 1314-1323.
13. Park, H., “Model-Based Optimization of Ultra High Performance Concrete Highway Bridge Girders,” Massachusetts Institute of Technology, 2003, 139 pp.
14. Soh, M., “Model-Based Design of a Ultra High Performance Concrete Prototype Highway Bridge Girder,” Massachusetts Institute of Technology, 2003, 64 pp.

15. AASHTO, *AASHTO LRFD Bridge Design Specifications*, *5th Edition*, American Association of State Highway and Transportation Officials, 2010.

16. Graybeal, B., “Structural Behavior of a 2nd Generation Ultra-High Performance Concrete Pi-Girder,” Federal Highway Administration, NTIS Accession No. PB2009-115496, 2009, 102 pp.

17. B. Graybeal, “UHPC making strides”, Public Roads, 72 (4), 17pp.

18. ABAQUS Software and Documentation, Version 6.11-1. © Dassault Systèmes, SIMULIA, 2011.

19. Chen, W. F., “Plasticity in Reinforced Concrete,” McGraw-Hill, Inc., 1982, 474 pp.

20. Hillerborg, A. M. Modeer, and P. E. Petersson, “Analysis of Crack Formation and Crack Growth in Concrete by Means of Fracture Mechanics and Finite Elements,” *Cement and Concrete Research*, V. 6, 1976, pp. 773-782.

21. Lee, J., and G.L. Fenves, “Plastic-Damage Model for Cyclic Loading of Concrete Structures,” *Journal of Engineering Mechanics,* V. 124, No.8, 1998, pp. 892–900.

22. Lubliner, J., J. Oliver, S. Oller, and E. Oñate, “A Plastic-Damage Model for Concrete,” *International Journal of Solids and Structures*, V. 25, No.3, 1989, pp. 229–326.

23. B. Graybeal, “Structural Behavior of a 2nd Generation Ultra-High Performance Concrete Pi-Girder,” Federal Highway Administration, NTIS Accession No. NTIS PB2009-115496, November 2009, 113 pp.

24. Graybeal, B., “Behavior of Field-Cast Ultra-High Performance Concrete Bridge Deck Connections Under Cyclic and Static Structural Loading,” Federal Highway Administration, NTIS Accession No. PB2011-101995, November 2010, 106 pp.